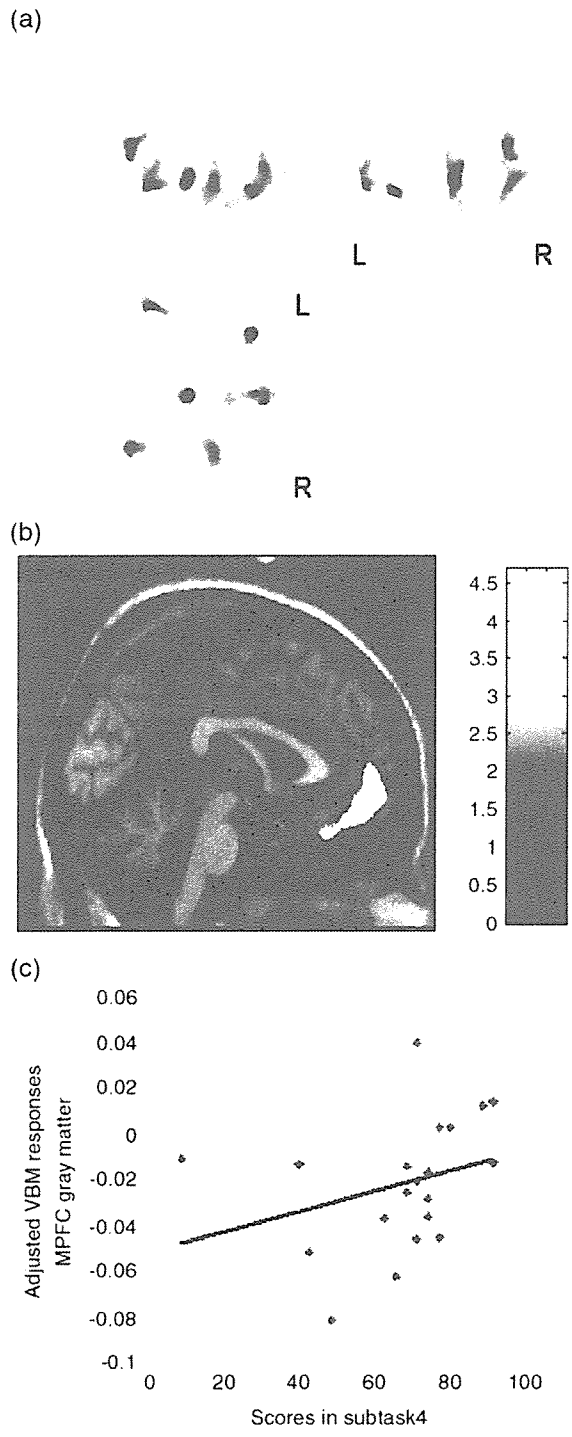

Fig. 2. (a) Gray matter concentration reductions in patients with schizophrenia were displayed on a glass brain. (b) Reduced concentration in the medial prefrontal cortex of patients with schizophrenia. (c) Adjusted concentration in the MPFC plotted against the scores in subtask 4 in patients with schizophrenia.

abscriable to the variation of the PIQ. However, such a possibility was eliminated because no significant correlation was found between the estimated PIQ scores and subtask 4 scores in the patients group (Spearman's $r=0.377$, $P>0.1$). No other relationship was observed between regional GMC's and PAT scores (all comparisons: $P>0.1$).

Discussion

This study mainly aimed to explore the relationship between regional gray matter abnormality and social cognition in individuals with schizophrenia. The results yielded three main findings.

First, the behavioral task revealed that the ability to attribute emotions to facial expressions and to the story protagonists is significantly compromised in schizophrenic patients. Impaired emotion recognition observed in subtask 2 is compatible with previous reports (Mandal et al., 1998). In contrast to several other studies (Johnston et al., 2001), intact processing of facial configurations in BFRT in our patients suggested that deficits in facial expression processing in schizophrenic patients are specific to the emotional component. Furthermore, it is possible that this is specific for certain negative emotions, with the greatest difficulty in recognizing fear, and to some extent, anger or sadness (Mandal et al., 1998; Edwards et al., 2002). Our results indicated that schizophrenic patients were less accurate than healthy participants in recognizing surprised and angry expressions. There was no significant difference between groups on fear identification, although fearful expressions were poorly recognized by schizophrenic patients, which might reflect the difficulty with which fearful expressions are recognized (Ekman and Friesen, 1976).

In subtasks 1, 3, and 4, the participants were presented with verbal or nonverbal scenarios depicting various social situations and were asked to identify the emotion of the main protagonists. The schizophrenic patients were markedly affected in these tasks; this is similar to the observations of previous studies in which various ToM-related tasks were repeatedly applied and defective ToM performances by schizophrenic patients were demonstrated (Brune, 2005). However, in contrast to the ToM tasks in the previous studies, which mainly examined cognitive mental attribution, i.e., intentions or beliefs, our tasks focused more on the emotional component of mental attribution, in other words, empathetic ToM. Indeed, some researchers have begun investigating the possible fractionation of functional requirements of cognitive ToM and empathetic ToM (Hynes et al., 2006; Vollm et al., 2006). However, these two aspects (i.e., ToM and empathy) do not have to be mutually distinctive but can also share some subcomponents. Notably, it was postulated that, a decoupling computational mechanism between self and other plays a critical role in both ToM and empathic understanding (Decety and Jackson, 2004; 2006). This would be further advanced by future studies. Based on the results of the present study, it appears likely that schizophrenic patients have more general deficits in representing the emotional states of others rather than a simple perceptual deficit in decoding emotional signals displayed by others.

The second finding of this study is the concentration reductions in the multiple frontal and temporal lobe structures, i.e., the MPFC, bilateral inferior frontal gyri, right anterior cingulate gyrus, left superior and middle temporal gyri, and right insula, in schizophrenic patients. In a recent meta-analysis of VBM studies conducted by Honea et al. (2005), reductions in the left superior and middle temporal gyri were most robustly observed in schizophrenic patients, followed by reductions in frontal lobes and insula, with which the present findings are consistent.

The third main finding of the present study is that among these abovementioned regions, we observed a specific association only between the MPFC abnormality and emotion-attribution deficit in schizophrenic patients. A number of neuroimaging and neuropsychological studies have indicated that the representation of mental states of others incorporates the MPFC (Brunet et al., 2000; Fletcher et al., 1995; Gallagher et al., 2000; Stone et al., 1998; Stuss et al., 2001; Vogeley et al., 2001). The relationship between the MPFC and emotion attribution in the present study would be in agreement with these earlier findings: the more pronounced the structural abnormalities of the MPFC, the greater is the impairment of the mentalizing ability. This view is also in line with the PET activation study that demonstrated abnormal activation within the MPFC during a ToM task in schizophrenic patients (Brunet et al., 2003).

However, as mentioned above, there appear to be functional and anatomical fractions in the ToM-related processes: cognitive ToM-attribution of cognitive states- and empathetic ToM-attribution of emotional states. These possible fractionations were directly investigated only very recently. Wider areas of activation in the MPFC in cognitive and empathetic ToMs have been demonstrated, using verbal (Hynes et al., 2006) or nonverbal scenarios (Vollm et al., 2006). Although some regions were activated in both the cognitive and the empathetic ToM, the ventral segments of the MPFC were activated strongly in the empathetic ToM. This region roughly corresponded to the abnormal concentration observed in the present study. Therefore, in contrast to the general mental attribution that is processed in the dorsal MPFC, the ventral sector could be associated with emotional components embedded in social interaction that would be particularly relevant to the empathetic aspects. Thus, based on the present findings, it may be speculated that the structural abnormalities of the ventral MPFC the possible key structure for the empathetic ToM underlie impaired emotional processes in real-life social interactive situations observed in schizophrenia.

The reason why only subtask 4 showed an association with the MPFC concentration clearly necessitates further investigation: nevertheless, one interpretation may be feasible. Although there appears to be general consensus that the MPFC plays a major role in social cognition, some authors assert that the role of the MPFC becomes particularly critical when the stimulus contains an explicit social context that can be directly identified (Vollm et al., 2006; Walter et al., 2004). Given that the same applies to the current findings, the photographs of actual social scenes used in subtask 4, which surpass subtasks 1 and 3 in explicitness or directness, may explain the selective association between this task and the MPFC abnormality.

The present study suggested only a weak association between clinical symptoms and the structural abnormalities. Further studies may discover a structure symptom relationship by categorizing the clinical symptoms in a more scrutinized manner such as in Liddle's tripartite model of schizophrenic symptomatology (Liddle, 1987). Another limitation of the present study is that we obtained a significant group difference in the analysis of GMC but not in that of GMV. These two analyses are considered to detect the different aspects of GM abnormalities (Good et al., 2001); thus, the reason why one analysis yielded a significant difference whereas the other did not need further investigation. Moreover, even though we found the interesting association between the MPFC and a social cognitive task, we did not correct it for multiple comparisons. Thus, we should take this conclusion as a preliminary one, though it would be expected for future studies by focusing on specific brain regions under specific hypothesis to verify the finding observed here. Finally, our tasks used static pictures as stimuli, but real-life social interactions are usually held in a dynamic way. Further experiments would be warranted to confirm the observed effect by using dynamic stimuli such as video-clips (Gross and Levenson, 1995) or moving faces (Yoshikawa and Sato, 2006).

In conclusion, the present study has exhibited a clear evidence of impaired social cognition in schizophrenia. Schizophrenic patients were impaired in attributing emotions not only to facial expressions but also to the story protagonists, which suggested general deficits in interpreting the emotional states of other people. Most importantly, it was demonstrated that the deficit in emotion attribution involving a social situation was correlated with concentration reductions in the MPFC of these patients. In this study, the possible link between social cognitive deficit and regional brain abnormality has been elucidated for the first time. This finding will help us to better characterize the nature of social dysfunctioning in schizophrenia and will further validate the neural basis of social cognition.

Acknowledgments

This research was supported by the Takeda Science Foundation, Uehara Memorial Foundation, Kobayashi Magobe Memorial Medical Foundation, Research Group for Schizophrenia, Japan, and a Research Fellowship of the Japan Society for the Promotion of Science.

References

Adolphs, R., Tranel, D., Damasio, H., Damasio, A., 1994. Impaired recognition of emotion in facial expressions following bilateral damage to the human amygdala. Nature 372 (6507), 669–672.

Antonova, E., Sharma, T., Morris, R., Kumari, V., 2004. The relationship between brain structure and neurocognition in schizophrenia: a selective review. Schizophr. Res. 70 (2–3), 117–145.

Ashburner, J., Friston, K.J., 2000. Voxel-based morphometry—the methods. NeuroImage 11 (6 Pt. 1), 805–821.

Baron-Cohen, S., Ring, H., Moriarty, J., Schmitz, B., Costa, D., Ell, P., 1994. Recognition of mental state terms. Clinical findings in children with autism and a functional neuroimaging study of normal adults. Br. J. Psychiatry 165 (5), 640–649.

Benton, A.L., Hamsher, K.S., Varney, N.R., Spreen, O., 1983. Facial Recognition: Stimulus and Multiple Choice Pictures. Oxford Univ. Press, New York.

Boik, R.J., 1981. A priori tests in repeated measures designs: effects of nonsphericity. Psychometrika 46 (3), 241–255.

Brothers, L., 1990. The social brain: a project for integrating primate behavior and neurophysiology in a new domain. Concepts Neurosci. 1, 27–51.

Brune, M., 2005. "Theory of mind" in schizophrenia: a review of the literature. Schizophr. Bull. 31 (1), 21–42.

Brunet, E., Sarfati, Y., Hardy-Baylé, M.C., Decety, J., 2000. A PET investigation of the attribution of intentions with a nonverbal task. NeuroImage 11, 157–166.

Brunet, E., Sarfati, Y., Hardy-Baylé, M.C., Decety, J., 2003. Abnormalities of brain function during a nonverbal theory of mind task in schizophrenia. Neuropsychologia 41, 1574–1582.

Darwin, C., 1872. The Expression of the Emotions in Man and Animals. Univ. of Chicago Press, Chicago.

Decety, J., Jackson, P.L., 2004. The functional architecture of human empathy. Behav. Cogn. Neurosci. Rev. 3 (2), 71–100.

Decety, J., Jackson, P.L., 2006. A social neuroscience perspective on empathy. Curr. Dir. Psychol. Sci. 15 (2), 54–58.

Edwards, J., Jackson, H.J., Pattison, P.E., 2002. Emotion recognition via facial expression and affective prosody in schizophrenia: a methodological review. Clin. Psychol. Rev. 22 (6), 789–832.

Ekman, P., Friesen, W., 1976. Pictures of Facial Affect. Consulting Psychologists Press, Palo Alto, CA.

Fletcher, P.C., Happe, F., Frith, U., Baker, S.C., Dolan, R.J., Frackowiak, R.S., Frith, C.D., 1995. Other minds in the brain: a functional imaging study of "theory of mind" in story comprehension. Cognition 57 (2), 109–128.

Gallagher, H.L., Happe, F., Brunswick, N., Fletcher, P.C., Frith, U., Frith, C.D., 2000. Reading the mind in cartoons and stories: an fMRI study of 'theory of mind' in verbal and nonverbal tasks. Neuropsychologia 38 (1), 11–21.

Genovese, C.R., Lazar, N.A., Nichols, T., 2002. Thresholding of statistical maps in functional neuroimaging using the false discovery rate. NeuroImage 15 (4), 870–878.

Good, C.D., Johnsrude, I.S., Ashburner, J., Henson, R.N., Friston, K.J., Frackowiak, R.S., 2001. A voxel-based morphometric study of ageing in 465 normal adult human brains. NeuroImage 14 (1 Pt. 1), 21–36.

Gross, J.J., Levenson, R.W., 1995. Emotion elicitation using films. Cogn. Emot. 9, 87–108.

Gur, R.E., Turetsky, B.I., Cowell, P.E., Finkelman, C., Maany, V., Grossman, R.I., Arnold, S.E., Bilker, W.B., Gur, R.C., 2000. Temporolimbic volume reductions in schizophrenia. Arch. Gen. Psychiatry 57 (8), 769–775.

Honea, R., Crow, T.J., Passingham, D., Mackay, C.E., 2005. Regional deficits in brain volume in schizophrenia: a meta-analysis of voxel-based morphometry studies. Am. J. Psychiatry 162 (12), 2233–2245.

Hornak, J., Rolls, E.T., Wade, D., 1996. Face and voice expression identification in patients with emotional and behavioural changes following ventral frontal lobe damage. Neuropsychologia 34 (4), 247–261.

Hynes, C.A., Baird, A.A., Grafton, S.T., 2006. Differential role of the orbital frontal lobe in emotional versus cognitive perspective-taking. Neuropsychologia 44 (3), 374–383.

Inagaki, A., 2004. Translation Table of Psychotropic Drugs. Keio University, Tokyo.

Johnston, P.J., Katsikitis, M., Carr, V.J., 2001. A generalised deficit can account for problems in facial emotion recognition in schizophrenia. Biol. Psychol. 58 (3), 203–227.

Kay, S.R., Fiszbein, A., Opler, L.A., 1987. The positive and negative syndrome scale (PANSS) for schizophrenia. Schizophr. Bull. 13 (2), 261–276.

Liddle, P.F., 1987. The symptoms of chronic schizophrenia. A re-examination of the positive–negative dichotomy. Br. J. Psychiatry 151, 145–151.

Mandal, M.K., Pandey, R., Prasad, A.B., 1998. Facial expressions of emotions and schizophrenia: a review. Schizophr. Bull. 24 (3), 399–412.

Pinkham, A.E., Penn, D.L., Perkins, D.O., Lieberman, J., 2003. Implications for the neural basis of social cognition for the study of schizophrenia. Am. J. Psychiatry 160 (5), 815–824.

Premack, D., Woodruff, G., 1978. Chimpanzee problem-solving: a test for comprehension. Science 202 (4367), 532–535.

Rau, J.C., 1993. Perception of verbal and nonverbal affective stimuli in complex partial seizure disorder [abstract]. Dissertation Abstracts Int B 54, 506B.

Sanfilipo, M., Lafargue, T., Rusinek, H., Arena, L., Loneragan, C., Lautin, A., Feiner, D., Rotrosen, J., Wolkin, A., 2000. Volumetric measure of the frontal and temporal lobe regions in schizophrenia: relationship to negative symptoms. Arch. Gen. Psychiatry 57 (5), 471–480.

Shenton, M.E., Dickey, C.C., Frumin, M., McCarley, R.W., 2001. A review of MRI findings in schizophrenia. Schizophr. Res. 49 (1–2), 1–52.

Stone, V.E., Baron-Cohen, S., Knight, R.T., 1998. Frontal lobe contributions to theory of mind. J. Cogn. Neurosci. 10 (5), 640–656.

Stuss, D.T., Gallup, G.G.Jr., Alexander, M.P., 2001. The frontal lobes are necessary for 'theory of mind'. Brain 124 (Pt. 2), 279–286.

Talairach, J., Tournoux, P., 1988. Co-Planar Stereotaxic Atlas of the Human Brain. Thieme, Stuttgart, Germany.

Vasey, M.W., Thayer, J.F., 1987. The continuing problem of false positives in repeated measures ANOVA in psychophysiology: a multivariate solution. Psychophysiology 24 (4), 479–486.

Vogeley, K., Bussfeld, P., Newen, A., Herrmann, S., Happe, F., Falkai, P., Maier, W., Shah, N.J., Fink, G.R., Zilles, K., 2001. Mind reading: neural mechanisms of theory of mind and self-perspective. NeuroImage 14 (1 Pt. 1), 170–181.

Vollm, B.A., Taylor, A.N., Richardson, P., Corcoran, R., Stirling, J., McKie, S., Deakin, J.F., Elliott, R., 2006. Neuronal correlates of theory of mind and empathy: a functional magnetic resonance imaging study in a nonverbal task. NeuroImage 29 (1), 90–98.

Walter, H., Adenzato, M., Ciaramidaro, A., Enrici, I., Pia, L., Bara, B.G., 2004. Understanding intentions in social interaction: the role of the anterior paracingulate cortex. J. Cogn. Neurosci. 16 (10), 1854–1863.

Yoshikawa, S., Sato, W., 2006. Enhanced perceptual, emotional, and motor processing in response to dynamic facial expressions of emotion. Jpn. Psychol. Res. 48 (3), 213–222.

原著

論文受付
2006年4月12日
論文受理
2006年6月22日
Code Nos. 333
523

二次元および三次元PET収集における雑音等価計数と再構成画像の画質の評価

松本圭一[1,2]・清水敬二[1]・北村圭司[3]
渡辺英治[1]・村瀬研也[2]・千田道雄[1]

1)先端医療センター分子イメージンググループ
2)大阪大学大学院医学系研究科保健学専攻医用物理工学講座
3)株式会社島津製作所医用機器事業部技術部

緒言

陽電子放出断層撮影装置(PET装置)にて計測される即発同時計数には，画像を構築する真の同時計数以外に偶発同時計数と散乱同時計数が含まれる．後者二つの計数は定量性だけでなく画質にも大きく影響するため，補正(減算)を行い定量性の高いPET画像を作成している．PET装置における画質評価は，受診者動作特性曲線を用いた観察者視覚評価もしばしば行われるが[1,2]，計数率から簡便に画質を推測できる雑音等価計数(noise equivalent count；NEC)[3,4]の方が広く用いられている．NECは偶発同時計数と散乱同時計数を考慮したPET計測における信号雑音(signal/noise；S/N)比の指標であり，次式で表される．

$$NEC = \frac{T^2}{T + S + (1+k)fR} \quad \cdots\cdots(1)$$

ここで，Tは真の同時計数，Sは散乱同時計数，Rは

Comparison of Noise Equivalent Count Rate and Image Quality for Two-dimensional and Three-dimensional PET Scans

Keiichi Matsumoto,[1,2] Keiji Shimizu,[1] Keishi Kitamura,[3] Eiji Watanabe,[1] Kenya Murase,[2] and Michio Senda[1]

1)Division of Molecular Imaging, Department of Image-based Medicine, Institute of Biomedical Research and Innovation
2)Department of Medical Physics and Engineering, Division of Medical Technology and Science, Course of Health Science, Graduate School of Medicine, Osaka University
3)R&D Department, Medical Systems Division, Shimadzu Corporation

Received April 12, 2006; Revision accepted June 22, 2006; Code Nos. 333, 523

Summary

The aim of this study was to investigate the correlation between noise equivalent count(NEC)rates and the signal-to-noise ratio(S/N)in reconstructed images. The NEC rates were determined using uniform 20 cm and 70 cm tall, 20 cm diameter cylinders filled with ^{11}C. The phantoms were scanned in both two-dimensional and three-dimensional modes. The reconstructed image noise was evaluated using FBP and OSEM algorithms(4 iterations and 8 subsets). The images were filtered to a final image resolution of 6.5 mm. From the reconstructed image sets, averages and standard deviations of images were generated, from which the average image S/N(=average/standard deviation)was calculated within an 18 cm central ROI. The S/N of a central slice and an end slice was compared with the NEC. The NEC was found to have a linear relationship to the image S/N of all slices, depending on differences in noise properties specific to the reconstruction algorithm. In two-dimensional mode, although the image S/N of the central slice and the edge slice showed a linear relationship with the NEC, in three-dimensional mode, the S/N of the central slice did not show a relationship with the NEC. The linear relationship was also found in both two- and three-dimensional acquisition modes, as well as for the different activity distributions. These results indicate that the NEC is not only a measure for comparing the count rate performance of imaging systems. However, an absolute evaluation is impossible to depend on reconstruction algorithm, slice number, and phantom type.

Key words: positron emission tomography (PET), noise equivalent count (NEC), image quality, filtered back projection (FBP), ordered subsets expectation maximization (OSEM)

別刷資料請求先：〒650-0047 神戸市中央区港島南町2丁目2番
先端医療センター 分子イメージンググループ 松本圭一 宛

偶発同時計数，fは被写体(ファントム)が断面内の有効視野内に占める割合である．kは偶発同時計数の補正方法に依存する係数であり，遅延同時計数回路により偶発同時計数を実測する場合は1となる．NECは偶発および散乱同時計数補正が適切に施されていることを前提とした指標であるが，計数率から簡便にS/N比を推測できるため物理学的性能評価[4]や全身検査の投与量決定[5]などに用いられている．

一方，近年のPET装置は感度を向上させるために，体軸方向視野の拡大や三次元収集を行って検出器受容立体角(幾何学的効率)を拡大させている．セプタを使用しない三次元収集は，視野全体の感度を飛躍的に向上させることが可能であるが，検出器最大リング差や体軸方向のline of responseの束ね(span)に依存して中央スライスよりも両端スライスの感度(計数率)が低下する[6]．加えて三次元収集は，視野外放射線が偶発および散乱同時計数となって定量性や画質を劣化させることが報告されている[7]．これは，偶発同時計数が一般に遅延同時計数回路によって補正されるためであり，(1)式分母における偶発同時計数の増加($2R$)にて説明できる．また市販のPET装置に広く標準装備されているシミュレーションベースの散乱補正法[8]は，厳密には視野外放射線による散乱同時計数に対応していないため，視野外放射線が多くなるほど定量性や画質の劣化が顕著になる．

NECを用いてS/N比を評価するためには，収集方法，視野外放射線さらには画像再構成法に依存することなく，低放射能濃度から高放射能濃度まで直線(相関)性が担保されている必要がある．加えて，視野全体の計数率からS/N比を推測するNECが，各画像スライスのS/N比と相関関係にあれば，さまざまな条件下における画質評価に用いることができると考えられる．本研究の目的は，収集方法，視野外放射線，放射能濃度および画像再構成法を変化させて，NECとPET画像のS/N比の関係を評価することである．

1．方　法

1-1　使用機器および測定方法

使用したPET装置はECAT EXACT HR+[9](SIEMENS社製)で，検出器リング間を隔てるセプタを出し入れすることで二次元および三次元収集が可能である．セプタの素材はタングステンであり，長さ66.5mm，厚み0.8mmである．4.39×4.05×30mmのBGO結晶を総計18,432個有し，スライス間隔2.4mmにて63画像スライス(32検出器リング)を撮像可能である．体軸方向の有効視野は15.5cmであり，視野中心における断面方向および体軸方向の空間分解能は，二次元収集がそれぞれ4.5mmと4.9mmであり，三次元収集は4.3mmと4.1mmである[9]．またエネルギーウィンド設定は350～650keVであり，トランスミッション用外部線源として^{68}Ge-^{68}Ga(initial activity：185MBq/本)線線源を3本有している．検出器最大リング差とspanは，二次元収集がそれぞれ7と15であり，三次元収集は22と9である．

PET測定は，^{11}C溶液を封入した20cmϕ×20cm(6283.2cm^3)と20cmϕ×70cm(21991.2cm^3)の円筒ファントムを用いた．PET装置の性能評価のための測定指針[10]に準拠して，高計数率特性(計数損失等の補正と精度とS/Nの比)の測定を二次元と三次元収集で行った．指針では，「計数損失および偶発同時計数が無視できるような計数率まで測定し，測定間隔は使用核種の半減期の1/2以下，かつ各フレームの測定時間は半減期の1/4以下とし，全体の測定は5半減期以上にわたってダイナミック測定を行う」としている．本研究ではファントム封入用に^{11}C溶液(半減期：20.4min)を封入したため，測定間隔および各フレームの測定時間を5分とした30フレームのダイナミック測定を行い，全体の測定時間は約5時間とした．二次元収集における測定開始時間でのファントム内放射能濃度は，20cmϕ×20cmファントムが757.1kBq/mlであり，20cmϕ×70cmファントムが357.0kBq/mlである．同じく三次元収集では，20cmϕ×20cmファントムが206.3kBq/mlであり，20cmϕ×70cmファントムが145.6kBq/mlである．またトランスミッション測定はファントム内に放射能がない状態で30分間測定した．

1-2　データ処理

すべての測定データは，計数損失補正，偶発同時計数補正(delayed coincidence correction)，散乱線補正(2D：deconvolution method[11]，3D：single scatter simulation algorithm[8])，および吸収補正を行った後，filtered back projection(FBP)法とordered subsets expectation maximization(OSEM)法を用いて画像再構成を行った．OSEM法における繰り返し回数とサブセット数は，臨床条件と同様にそれぞれ4と8を選択した[12]．平滑化フィルタにはGaussianフィルタ(6mm FWHM)を使用し，マトリックスサイズは128×128，ボクセルサイズは2.6×2.6×2.4mmとした．また，三次元収集されたエミッションデータは，Fourier rebinning法[13]にて近似的に二次元データに変換した．

1-3　データ解析

1-3-1　NECの算出

PET画像は即発同時計数から偶発同時計数と散乱同時計数を補正して画像を作成するため，それらが全くない理想的な場合の画像と比較してS/N比は低下す

Table Reported JIRA 1994 performance characteristics for PET scanner.

	2-dimensional	3-dimensional
Scatter fraction of System (%)	19	37

る．NECは，それらS/N比を劣化させる計数率を考慮して画質を推測する指標である．

2種類の異なるファントムにおける二次元および三次元収集のNECは(1)式を用いて算出した．偶発同時計数は遅延回路により実測した値を用いたため，(1)式におけるkを1とした．断面内の有効視野が65.3cmであるためファントムが占める割合(f)は0.31とし，真の同時計数は次式を用いて算出した．

$$T=(T+S)\times(1-scatter\ fraction) \quad \cdots\cdots\cdots\cdots\cdots\cdots(2)$$

散乱フラクションは，均一な放射能濃度を持つ円筒ファントムに対する散乱同時計数の割合である．PET装置の性能評価のための測定指針[10, 14]に準拠して20cmϕ×20cmファントムを用いてあらかじめ測定した値を用いた(Table)．

1-3-2 PET画像のS/N比

各フレームにおける各画像スライスの中心に18cmの円形関心領域を設定し，その画像放射能濃度の平均値と標準偏差から次式を用いてPET画像のS/N比を算出した．

$$Image\ noise(S/N)^2=\left(\frac{average}{standard\ deviation}\right)^2 \quad \cdots\cdots(3)$$

本研究では，全63画像スライスの平均S/N比のほかに，中央10スライスと両端5スライス(計10スライス)の平均S/N比も算出し，それぞれ最大NECまでの計数率と比較を行った．加えて，最大NECにおける各スライスのS/N比を比較した．

2．結　果

二次元および三次元収集における各ファントムのNECをFig. 1とFig. 2に示す．二次元収集におけるNECは，両ファントムともに30kBq/ml以上の放射能濃度から緩やかに低下したが(Fig. 1)，三次元収集におけるNECは，20cmϕ×20cmファントムでは約12kBq/ml以上で，20cmϕ×70cmファントムでは約6kBq/ml以上の放射能濃度で急激に低下した(Fig. 2)．20cmϕ×20cmファントムおよび20cmϕ×70cmファントムにおける最大NEC(放射能濃度)は，二次元収集でそれぞれ29.4kcps(45.9kBq/ml)と11.3kcps(21.6kBq/ml)であり，三次元収集では79.2kcps(12.5kBq/ml)と27.3kcps(6.3kBq/ml)であった．また両収集ともに20cmϕ×70cmファントムの方がすべての放射能濃度でNECが低値であった．

二次元収集におけるNECとS/N比の関係をFig. 3とFig. 4に示す．直線は全63画像スライスの平均S/N比における回帰曲線である．20cmϕ×20cmファントムおよび20cmϕ×70cmファントムともにNECとPET画像のS/N比はほぼ比例(直線)関係を示したが，最大NEC付近では直線関係を示さなかった．また20cmϕ×70cmファントムにおけるFBP法のS/N比が最も低値であった．FBP法およびOSEM法ともにNECが高値になるほど，中央スライスと両端スライスのS/N比に差を認めた．また両ファントムとも，すべてのNECでOSEM法のS/N比が高値であり，20cmϕ×70cmファントムではその差が顕著であった．

三次元収集におけるNECとS/N比の関係をFig. 5とFig. 6に示す．Fig. 3およびFig. 4と同様に，直線は全63画像スライスの平均S/N比における回帰曲線である．三次元収集においても，二次元収集と同様に最大NEC付近でS/N比のバラツキが大きかった．FBP法における全63画像スライスのS/N比は，両ファントムともにNECと良好な直線関係を示したが，中央スライスのS/N比は直線性が不良であった．またOSEM法においては，両ファントムとも両端スライスのS/N比以外は直線関係が不良であり，中央スライスのS/N比は10kcps以上のNECで直線性が不良であった．

Fig. 7に最大NECにおけるFBP法の各スライスのS/N比を示す．二次元収集における20cmϕ×70cmファントムのS/N比が最も低値であった．また三次元収集では，収集の物理的特性および視野外放射線の影響を受けて，両端スライスのS/N比が低下する傾向にあった．

3．考　察

NECは放射能分布が均一ファントムを用いて画質を推測できるため汎用されている．しかしながら，使用するファントムの長さ(視野外放射線)や大きさ，さらには収集方法に依存して偶発同時計数や散乱同時計数が異なり[15]，加えて再構成法(再構成パラメータ)に依存して画質が異なるため[16]，NECと画質に相関性を示すかは不明である．一方，計測学において統計雑音すなわち標準偏差を正確に評価するためには同一条件化で複数回の測定が必要であるが[17]，PET計測においては非常に難しい測定となる．そこで本研究では，関心領域内の画素値の標準偏差がPET画像の統計雑音に比

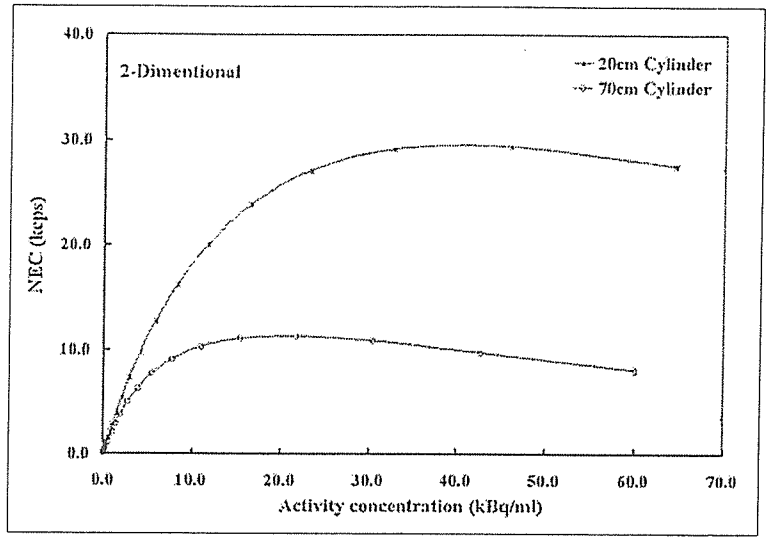

Fig. 1 NEC for the 20 cm and 70 cm tall cylinders, acquired in two-dimensional mode.

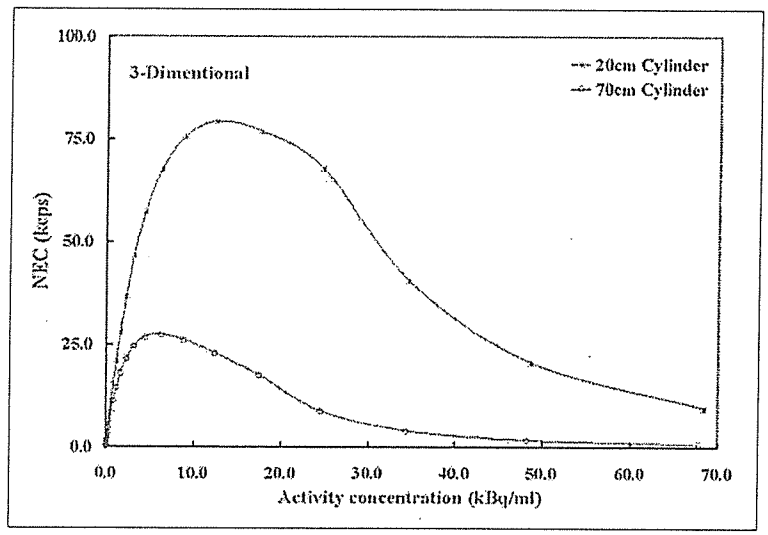

Fig. 2 NEC for the 20 cm and 70 cm tall cylinders, acquired in three-dimensional mode.

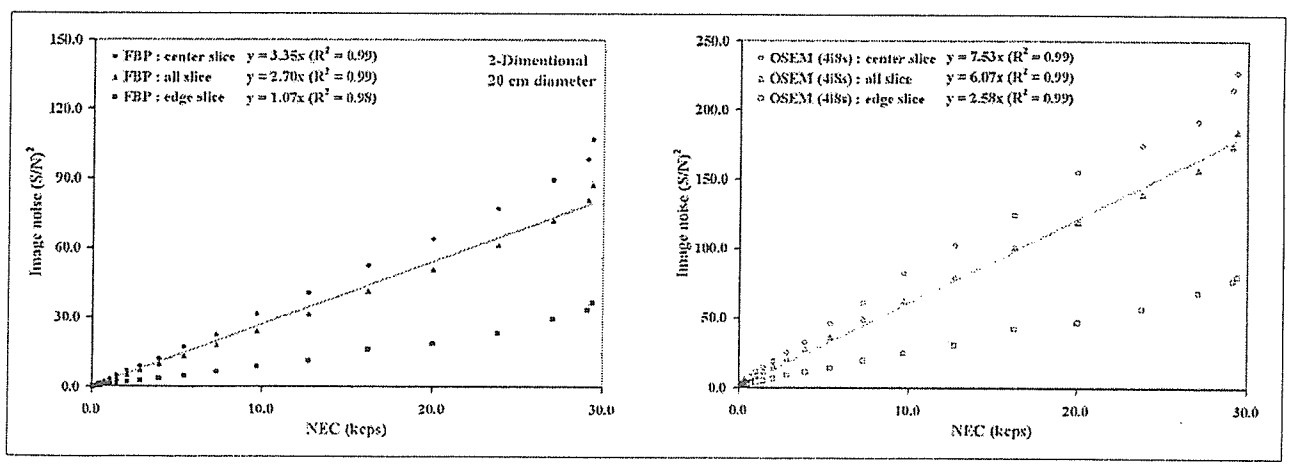

Fig. 3 Corresponding image noise $(S/N)^2$ plotted against NEC for 20 cm tall cylinders, where the image reconstructed FBP (a) and OSEM $4i8s$ (b), acquired in two-dimensional mode. Data points of all slices approach a straight line.

a | b

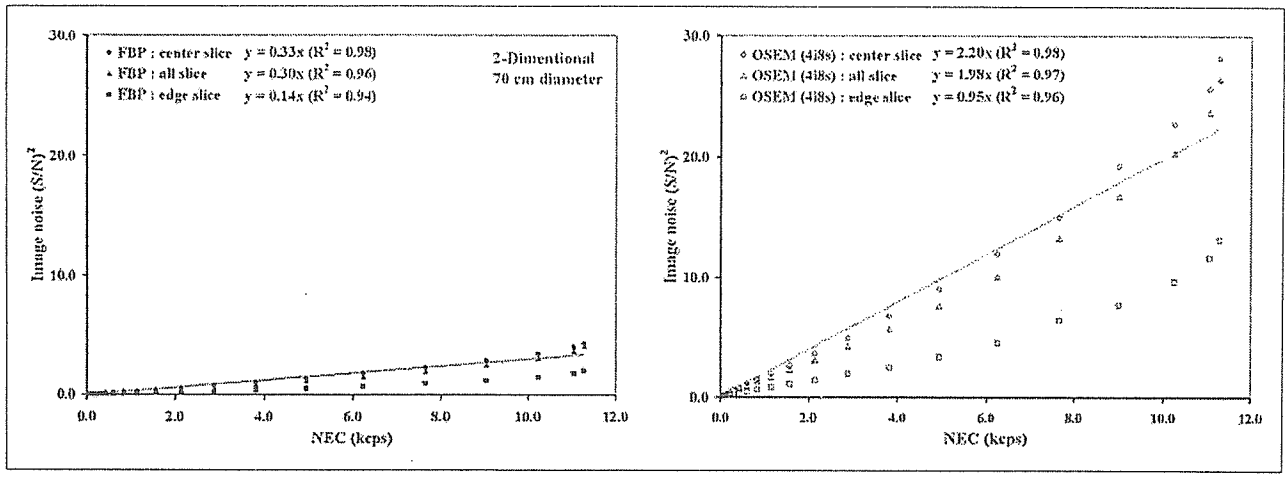

Fig. 4 Corresponding image noise $(S/N)^2$ plotted against NEC for 70 cm tall cylinders, where the image reconstructed FBP (a) and OSEM $4i8s$ (b), acquired in two-dimensional mode. Data points of all slices approach a straight line.

a | b

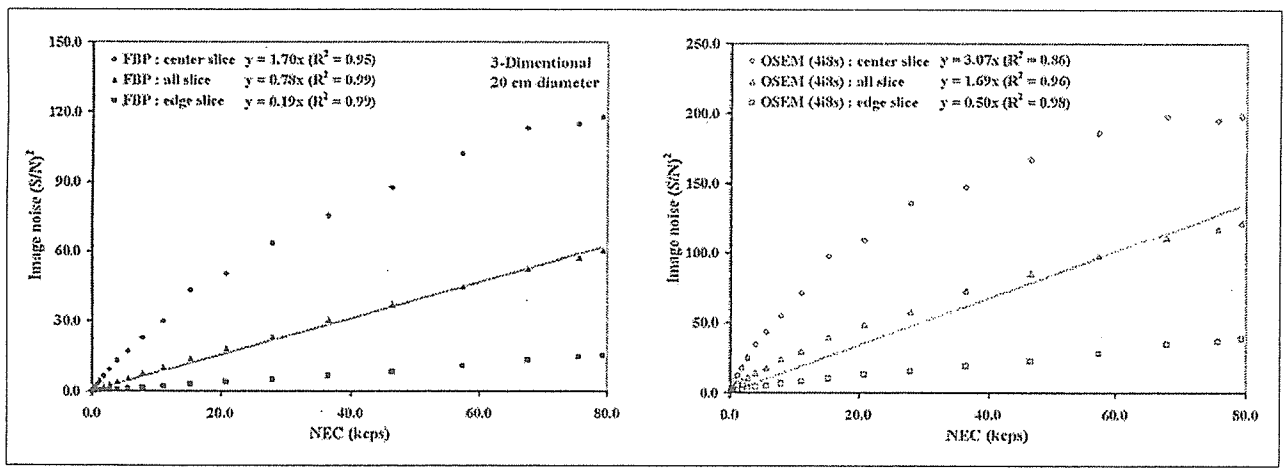

Fig. 5 Corresponding image noise $(S/N)^2$ plotted against NEC for 20 cm tall cylinders, where the image reconstructed FBP (a) and OSEM $4i8s$ (b), acquired in three-dimensional mode. Data points of all slices approach a straight line.

a | b

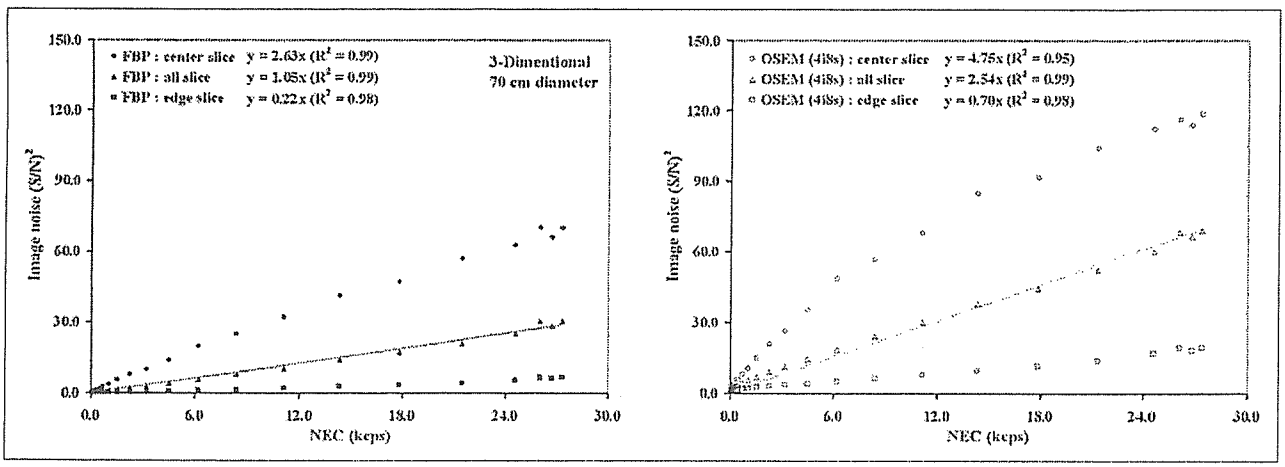

Fig. 6 Corresponding image noise $(S/N)^2$ plotted against NEC for 70 cm tall cylinders, where the image reconstructed FBP (a) and OSEM $4i8s$ (b), acquired in three-dimensional mode. Data points of all slices approach a straight line.

a | b

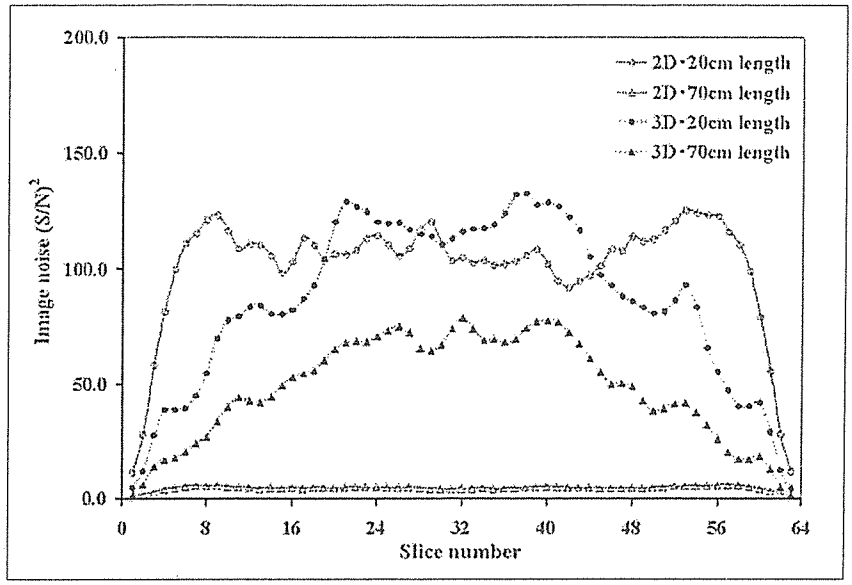

Fig. 7 Comparison of image noise for peak NEC acquired in two- and three-dimensional mode. All images were reconstructed by FBP.

例すると仮定し，さまざまな条件下でNECとPET画像のS/N比を評価した．

三次元収集のNECだけでなく，二次元収集におけるNECも視野外放射線の影響を強く受けた(Fig. 1，2)．二次元収集であっても視野外放射線が存在する場合には，PET装置のセプタ厚や，各検出器とファントムとの幾何学的効率に依存して偶発同時計数は増加する．言い換えると，視野外放射線が存在しない場合に真の同時計数として計測される事象も，視野外放射線の存在によって偶発同時計数として計測されてしまい，偶発同時計数の増加だけでなく真の同時計数の減少をきたす．二次元収集の利点は散乱および偶発同時計数が少ないことであるが，欠点として真の同時計数も少ない．このため視野外放射線の存在に起因する真の同時計数の減少がNECに大きく影響したと考えられる．

三次元収集において，20cmϕ×20cmファントムでは約7kBq/ml以上で，20cmϕ×70cmファントムでは約13kBq/ml以上の放射能濃度でNECの低下を認めた(Fig. 2)．これは偶発同時計数と散乱同時計数の増加およびそれに伴うPET装置と収集コンピュータにおけるデータ転送の飽和が原因であると考えられる．データ転送の飽和は，検出器の種類や信号処理回路などに依存するが，高いNECを獲得する放射能の濃度幅が小さいため臨床検査においては投与放射能量の最適化が非常に重要であると考える．しかしながら，ファントム実験(20cmϕ×70cmファントム)にて最大NECを得る放射能濃度は人体における最適投与量とならない[5, 18]．これは被検者の放射能分布や散乱体が一様でないためであり，使用核種，体内分布および撮像部位を考慮すれば，より低い放射能濃度が人体における最適投与量になると考える．

二次元収集における20cmϕ×20cmファントムのS/N比は，両画像再構成法とも広い範囲で良好な直線関係を示した(Fig. 3)．またPET収集の物理特性を反映して中央スライスは高いS/N比を，両端スライスは低いS/N比を示した．しかしながら，その直線性は最大値NECの90％程度までであり，最大NEC付近ではすべての条件において(Fig. 3〜6)バラツキを認めた．これは高放射能濃度におけるパルスパイルアップ現象[19]のためと考える．すなわち，二つ以上のγ線が一つのブロック検出器にほぼ同時に入射して，検出器(光電子増倍管)の信号パルスが重なり合い，位置やエネルギー情報のミスコーディングを生じて最終的に検出器の感度ムラをきたしたと考えられる．また，FBP法におけるS/N比がOSEM法と比較して約1/2倍低値を示したのは，画素値に負の値を有しているためバラツキ(標準偏差)が大きくなったことが原因と考えられ，画像再構成法の特徴を表した結果であると考える[20]．一方，20cmϕ×70cmファントムのS/N比は，前述の結果(Fig. 3)と同様に最大NECの90％程度まで直線性を認めたが，FBP法では顕著にS/N比が低値であった(Fig. 4a)．NECが10kcps未満(Fig. 1)，すなわち低計数率では逐次近似画像再構成法(OSEM法)が有用であると考えられた．また，二次元収集におけるNECと全63画像スライスおよび中央スライスのS/N比は，ほぼ同等の傾きを保つ回帰式で表すことが可能であった．これは二

次元収集における視野内の真の同時計数が比較的均等に各スライスに分配されるためであり，各画像スライスのS/N比が広い範囲で均一であったことからも説明できる(Fig. 7)．したがって，二次元収集ではNECを用いて全画像スライスのS/N比および中央スライスのS/N比を推測可能であると考える．

三次元収集における両ファントムの全63画像スライスおよび両端スライスのS/N比は，二次元収集と同様に最大NECの90％程度まで良好な直線関係を示したが，中央スライスのS/N比のみ直線性が不良であった(Fig. 5, 6)．三次元収集は収集の特性上，視野外放射線源の有無にかかわらず中央スライスの計数率，すなわち真の同時計数と偶発同時計数が両端スライスよりも高くなる．本研究で使用した偶発同時計数補正は，即発同時計数からリアルタイムに差し引く方法であり，差分によって真の同時計数の統計ノイズが増大する特徴を有している．このため，高NECでは多くの偶発同時計数を減算することになり，結果としてNECとS/N比が直線関係を示さなかったと考える．高NECすなわち偶発同時計数が多い場合には，遅延同時計数を別の収集メモリに収集しておき，測定終了後に適当な平滑化処理やノイズ低減処理を施したのち減算処理を行う方法[21]が有効であると考えられた．また三次元収集におけるNECは，前述の理由から全画像スライスの平均的なS/N比を推測していると考えられた．

高いS/N比のPET計測を行うためには，PET装置の感度や投与量を増加させることが一般的であるが，(1)式に示すようにTの増加をSやRの増加で相殺せぬようにPET計測しなければならない．散乱同時計数は被写体の大きさ(断面積)に依存するが，視野外放射線が存在する場合には正確に偶発同時計数と分離することは不可能であるため散乱フラクションは大きくなる[22]．偶発同時計数補正によるノイズの増加を抑制することも重要であるが，視野外放射線を考慮した新しい散乱補正法[23]を適用することでさらに画質は向上すると考える．NECは真の同時計数，偶発同時計数および散乱同時計数を考慮したPET計測における有効な画質推測指標である．しかしながら，偶発および散乱同時計数補正の精度およびPET収集のスライス感度特性に影響することに十分注意する必要がある．

4．結　語

収集方法および視野外放射線を変化させて，NECから画質を評価できるか検討を行った．二次元および三次元収集におけるNECは，全画像スライスの平均的な画質を評価する指標であった．また，視野外放射線の影響すなわち偶発同時計数の増加は画質と密接な関係にあるため補正方法の選択が重要であると考えられた．加えて三次元収集における中央スライスのS/N比はNECと直線関係を示さないため，NECを用いた画質評価は注意が必要であると考えられた．

本論文の要旨は第45回日本核医学学会総会(2005年11月，東京)にて発表した．

参考文献

1) Glatting G, Werner C, Reske SN, et al.: ROC analysis for assessment of lesion detection performance in 3D PET: influence of reconstruction algorithms. Med Phys, 30(9), 2315-2319,(2003).
2) Farquhar TH, Llacer J, Sayre J, et al.: ROC and LROC analyses of the effects of lesion contrast, size, and signal-to-noise ratio on detectability in PET images. J Nucl Med, 41(4), 745-754,(2000).
3) Strother SC, Casey ME, and Hoffman EJ: Measuring PET scanner sensitivity: relating countrates to image signal-to-noise ratios using noise equivalents counts. IEEE Trans Nucl Sci, 37(2), 783-788,(1990).
4) Nat. Elect. Manufacturers Assoc.: NEMA Standards Publ. NU 2-2001-Performance Measurements of Positron Emission Tomographs. Rosslyn, VA,(2001).
5) Watson CC, Casey ME, Bendriem B, et al.: Optimizing injected dose in clinical PET by accurately modeling the counting-rate response functions specific to individual patient scans. J Nucl Med, 46(11), 1825-1834,(2005).
6) Spinks TJ, Miller MP, Bailey DL, et al.: The effect of activity outside the direct field of view in a 3D-only whole-body positron tomograph. Phys Med Biol, 43(4), 895-904,(1998).
7) Watson CC, Newport D, Casey ME, et al.: Evaluation of simulation-based scatter correction for 3-D PET cardiac imaging. IEEE Trans Nucl Sci, 44(1), 90-97,(1997).
8) 楠岡英雄，西村恒彦，監修：5 PET．日本エム・イー学会編　核医学イメージング．pp.118-159，コロナ社，東京，(2001)．
9) Adam LE, Zaers J, Ostertag H, et al.: Performance evaluation of the whole-body PET scanner ECAT EXACT HR+ following the IEC standard. IEEE Trans Nucl Sci, 44(3), 1172-1179,(1997).
10) 日本アイソトープ協会　医学・薬学部会　サイクロトロン核医学利用専門委員会　核医工学ワーキンググループ：PET装置の性能評価のための測定指針．Radioisotopes，43(9)，115-135，(1994)．
11) Bergström M, Eriksson L, Bohm C, et al.: Correction for scattered radiation in a ring detector positron camera by integral transformation of the projections. J Comput Assist Tomogr, 7(1), 42-50,(1983).
12) 松本圭一，松浦　元，簑田英理，他：三次元全身FDG-PET収集におけるBody Mass Indexを用いた投与量および収集時間の最適化．日放技学誌，60(11)，1564-1573，(2004)．
13) Defrise M, Kinahan PE, Townsend DW, et al.: Exact and approximate rebinning algorithms for 3D-PET data. IEEE Trans Med Imaging, 16(2), 145-158,(1997).
14) 松本圭一，和田康弘，松浦　元，他：PET装置におけるLine of Responseを考慮した新しい雑音等価係数指標の評価．日放技学誌，60(8)，1116-1122，(2004)．
15) 山本誠一，三浦修一，飯田秀博，他：PETの3次元収集における被検体の形状と計数率特性の関係．核医学，33(4)，435-441，(1996)．
16) 大西英雄，木田哲生，篠原広行，他：SPECTの再構成法に関する研究班報告．日放技学誌，59(10)，1229-1247，(2003)．
17) 山田勝彦，野原弘基：第7章　計数値の統計的取扱い．日本放射線技術学会編　診療放射線技術学大系一専門技術学系13放射線計測学．pp.179-186，通商産業研究社，(1981)．
18) Badawi RD, Adam L-E, and Zimmerman RE: A simulation-based assessment of the revised NEMA NU-2 70-cm long test phantom for PET. In: Nuclear Science Symposium and Medical Imaging Conference Record. San Diego: IEEE; M6-6,(2001).
19) Germano G, and Hoffman EJ: A study of data loss and mispositioning due to pileup in 2-D detectors in PET. IEEE Trans Nucl Sci, 37(2), 671-675,(1990).
20) 松本圭一，和田康弘：Positron Emission Tomographyにおける低カウント領域でのFBP法とOS-EM法の比較．核医学技術，23(3)，191-198，(2003)．
21) Casey ME, and Hoffman EJ: Quantitation in positron emission computed tomography: 7. A technique to reduce noise in accidental coincidence measurements and coincidence efficiency calibration. J Comput Assist Tomogr, 10(5), 845-850,(1986).
22) Herzog H, Tellmann L, Hocke C, et al.: NEMA-NU2-2001 guided performance evaluation of four Siemens ECAT-PET scanners. IEEE Trans Nucl Sci, 51(5), 2662-2669,(2004).
23) Ferreira NC, Trebossen R, Lartizien C, et al.: A hybrid scatter correction for 3D PET based on an estimation of the distribution of unscattered coincidences: implementation on the ECAT EXACT HR+. Phys Med Biol, 47(9), 1555-1571,(2002).

図表の説明

Fig. 1　二次元収集におけるNECと放射能濃度の関係
Fig. 2　三次元収集におけるNECと放射能濃度の関係
Fig. 3　20cmϕ×20cm円筒ファントムを用いた二次元収集におけるNECと画質の関係：FBP法(a)とOSEM法(b)
直線は全画像スライスにおける回帰直線.
Fig. 4　20cmϕ×70cm円筒ファントムを用いた二次元収集におけるNECと画質の関係：FBP法(a)とOSEM法(b)
直線は全画像スライスにおける回帰直線.
Fig. 5　20cmϕ×20cm円筒ファントムを用いた三次元収集におけるNECと画質の関係：FBP法(a)とOSEM法(b)
直線は全画像スライスにおける回帰直線.
Fig. 6　20cmϕ×70cm円筒ファントムを用いた三次元収集におけるNECと画質の関係：FBP法(a)とOSEM法(b)
直線は全画像スライスにおける回帰直線.
Fig. 7　最大NECにおける二次元および三次元収集の各スライスの画質
すべての画像はFBPを用いて画像再構成を行った.

Table　(社)日本アイソトープ協会：PET装置の性能評価のための測定指針で評価されたPET装置の性能

Development of a Flexible End-Shield Using Tungsten Curtains for 3D PET

S. Yamamoto, *Member, IEEE*, S. Sakamoto, K. Matsumoto, and M. Senda, *Member, IEEE*

***Abstract*—In the three-dimensional (3D) acquisition of positron emission tomograph (PET) without septa, random and scatter due to events from outside the field of view (FOV) become a serious problem. They decrease the signal to noise ratio and the quantitation of the image and also limit the count rate capability of the PET system. To reduce these effects, we developed a flexible end-shield using tungsten curtains (curtain-shield) that consists of a mobile stand, a cylindrical support, and flexible tungsten curtains. The tungsten curtains are made of four layers of 30 mm square, 1 mm thick tungsten plates contained in pockets of cloth. Because the tungsten curtains are flexible, they can safely be used even in body studies. Reduction of random and scatter were observed by using the curtain-shield in both phantom and human studies. Results indicate that the curtain-shield has a potential to improve the image quality of PET studies.**

***Index Terms*—End-shield, flexible, positron emission tomography (PET), tungsten.**

I. Introduction

In the three-dimensional (3D) acquisition of positron emission tomograph (PET) without septa, random and scatter due to events from outside the field of view (FOV) become a serious problem. They decrease the signal to noise ratio and the quantitation of images and also limit the count rate capability. One solution to decrease these out-of-FOV events is the use of a fixed end-shield [1]–[3]. However, the shield decreases the diameter of the patient port of the PET scanner and has some difficulties in whole-body studies. Another solution is to use a fixed body-shield [4]–[6]. Although a body-shield can be used for whole body scanning, it needs modifications on the bed. Because the height of the body-shield is shorter than the diameter of the patient port, its use needs more caution to the subject during scanning. To overcome these limitations on fixed-shields, we developed a flexible end-shield using tungsten curtains called curtain-shield.

II. Materials and Methods

In Fig. 1, we show a schematic drawing of a curtain-shield attached to a PET scanner. The curtain-shield consists of a mobile stand, a cylindrical support, and flexible tungsten curtains made of tungsten plates contained in pockets of cloth. They are hung from a cylindrical support. Because the tungsten plates are separated from each others, the curtain-shield is so flexible that subject can be safely moved into or out of the patient port with minimum or no gap between subject and the tungsten curtain.

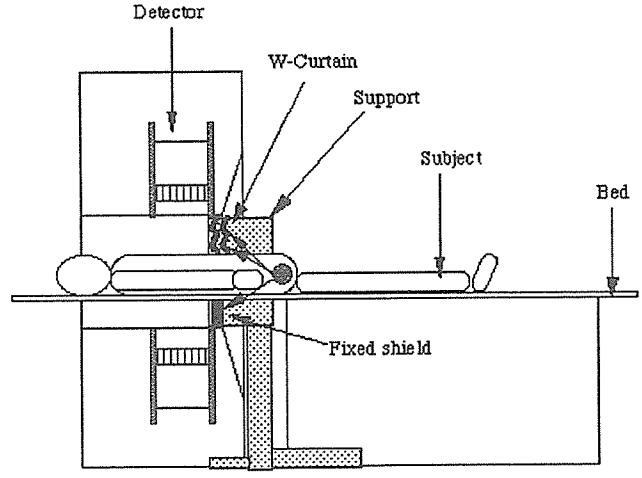

Fig. 1. Schematic drawing of developed shield using tungsten (W) curtains.

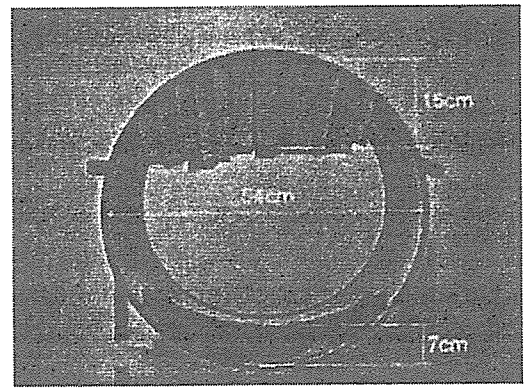

Fig. 2. Photograph of curtain-shield observed from one end of the cylindrical support.

In Fig. 2, we show a photograph of the curtain-shield taken from one end of the cylindrical support. The curtain-shield was designed for CTI EXACT 47 or EXACT HR+ PET scanner. The PET scanner used for the experiments has a ring diameter of 82 cm and patient port of 56 cm. The PET scanner has relatively long (~13 cm) internal fixed end-shields at both sides of the edges of the axial FOV.

The inside diameter of the cylindrical support was 54 cm, slightly smaller than the patient port of the PET scanner. From the upper inside of the cylindrical support, tungsten plates were hung. The size of a single tungsten plate was 30 mm × 30

Manuscript received July 14, 2005; revised March 28, 2006. This work was supported in part by a fund for the Development Program of New Medical Instruments, Kobe City.

S. Yamamoto is with the Kobe City College of Technology, Nishi-ku, Kobe 651-2194, Japan (e-mail: s-yama@kobe-kosen.ac.jp).

S. Sakamoto, K. Matsumoto, and M. Senda are with the Institute of Biomedical Research and Innovation (IBRI), Chuo-ku, Kobe 650-0047, Japan.

Color versions of Figs. 2–6 available online at http://ieeexplore.ieee.org.

Digital Object Identifier 10.1109/TNS.2006.876001

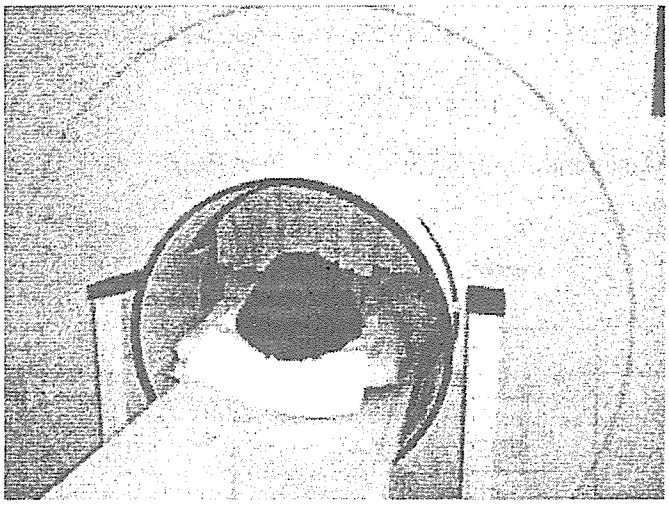

Fig. 3. Photograph of developed curtain-shield with subject.

mm × 1 mm, hung in four layers (4 mm) that absorb approximately 70% of the 511 keV gamma photons. There are some spaces between pockets for the tungsten plates. The maximum length (vertical height) of the curtain-shield was 15 cm.

Also an additional fixed end-shield was inserted in the gap below the bed because this does not disturb patients. The height of the fixed end-shield was 7 cm at maximum, 40 cm wide, and 5 mm thick (4 mm lead plus 1 mm stainless steel). The patient port in the vertical direction was reduced to 32 cm due to the upper and lower shields that may limit the size of the patients. A mobile stand is used to replace the curtain-shield when it is not used.

Fig. 3 shows a developed curtain-shield with a subject. When the curtain-shield touches the subject, it can bend without harming the patient.

III. Results

A. Phantom Experiments

First, we measured the random and scatter rates for a cylindrical phantom positioned out-of-FOV to evaluate the rejection capability of the curtain-shield for these events. A PET scanner, CTI EXACT 47, was used for all of the measurements. The lower energy threshold of the PET scanner was set to 350 keV.

Using a 20 cm diameter, 20 cm height cylindrical phantom that contained 20 MBq of Ge-68, random and scatter rates were measured as a function of the distance between the edge of the axial FOV of the PET scanner and the phantom. The arrangement of the phantom is shown in Fig. 4(A).

Measurements were made with and without the curtain-shield. Because no radioactivity was positioned in the FOV, the prompt minus delay rate measured by PET scanner was identified as scatter rate. An experiment with only a phantom outside the field of view will not necessarily reflect the rejection capability of the shielding for random coincidences since it shows only random coincidences between singles that both arose from activity outside the scanner. Extra random coincidences associated with out-of-FOV activity are, however, more likely between a single from activity within the scanner and a single from activity outside the scanner. The measurement is more a reflection of the reduction of outside singles with the shield.

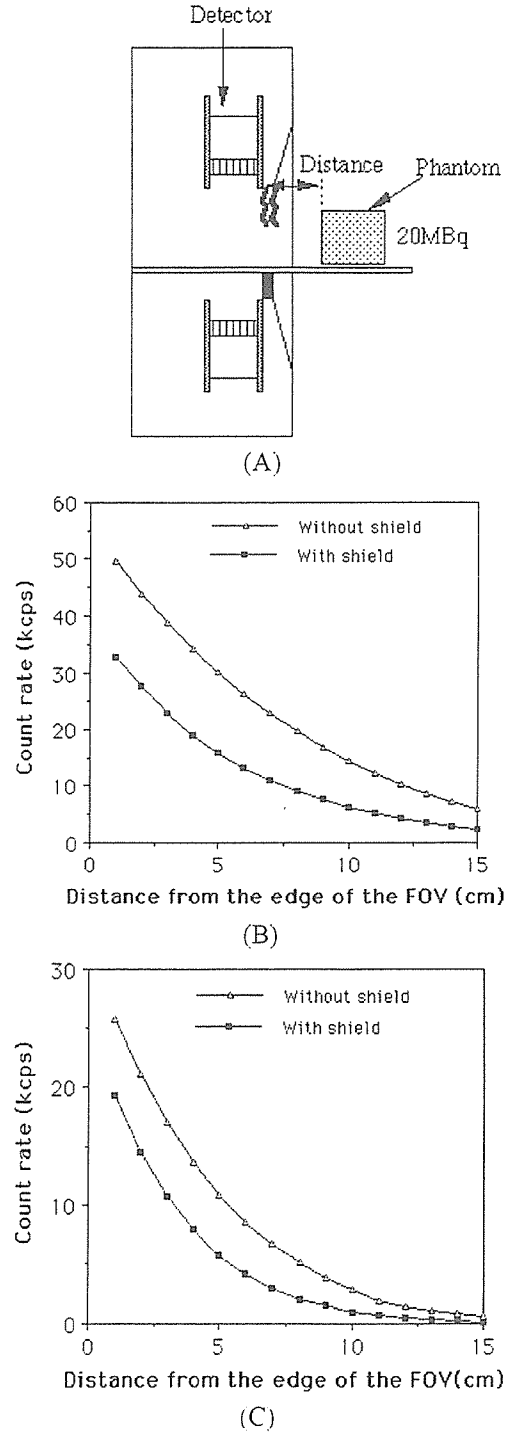

Fig. 4. Experimental set-up for random and scatter rates for phantom positioned out-of-FOV (A), random rate (B), and scatter rate (C) with and without the curtain-shield for a 20 cm diameter, 20 cm height cylindrical phantom positioned out-of-FOV.

Figs. 4(B) and (C) show random and scatter rates as a function of the distance from the edge of the FOV. Using the curtain-shield, random rate decreased 35%–60% and scatter rate decreased 25%–65% depending on the position of the phantom.

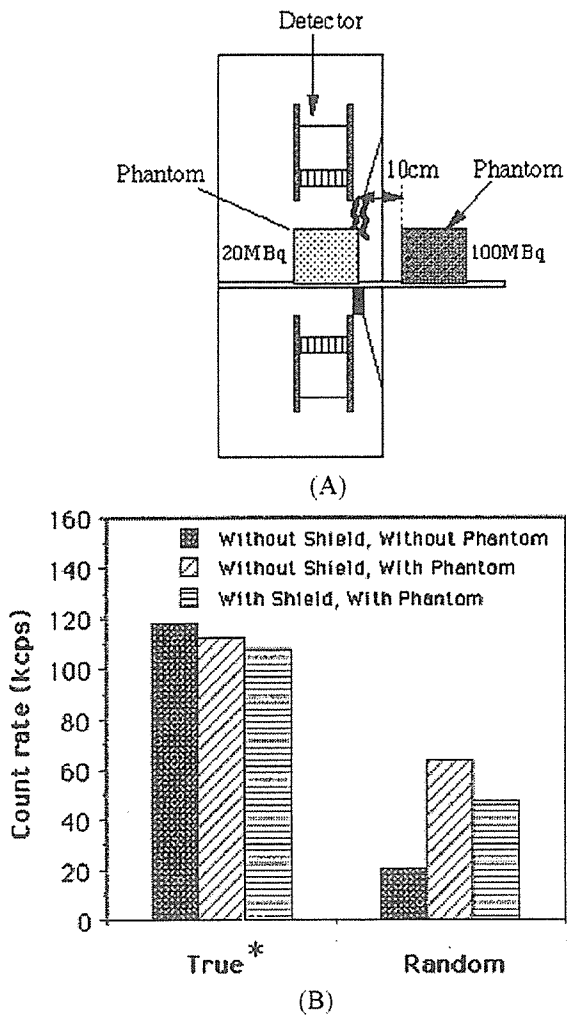

Fig. 5. Experimental set-up of phantoms positioned in FOV and out-of-FOV (A), true* ((B)-left), and random ((B)-right) count rates with and without the curtain-shield.

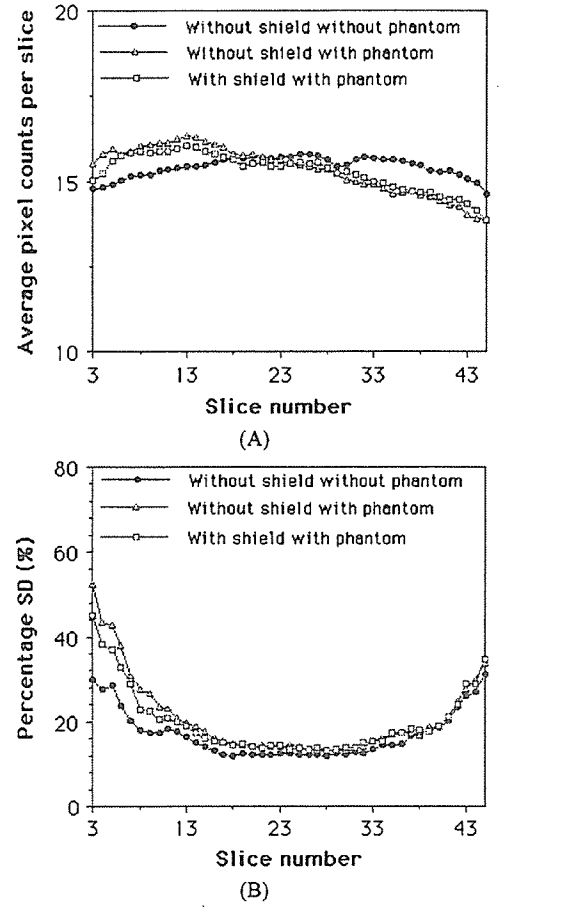

Fig. 6. Average pixel counts (A) and %SD (B) for each slice with phantom of 20 MBq in the FOV and another phantom of 100 MBq with and without positioned out-of-FOV.

Next, we measured the prompt minus delay and random rates with two 20 cm diameter, 20 cm long phantoms. One, containing 20 MBq, was placed in the scanning field, and another, containing 100 MBq, was placed 10 cm from the edge of the FOV. The phantom arrangement of this experiment is shown in Fig. 5(A). This measurement was intended to simulate human body study in which the large amount of radioactivity exists out-of-FOV. Measurements were made with and without the curtain-shield.

Results are shown in Fig. 5. In this figure, true* is the prompt minus delay rate, which is equivalent to the true plus scatter rate. Using the curtain-shield, true* rate slightly decreased probably because of the decrease of the scatter from the out-of-FOV phantom. The random rate decreased 25% by using the curtain-shield. In this experiment, true* rates decreased with the out-of-FOV phantom both with and without the curtain-shield. This probably reflects the deadtime from the out-of-field activity.

We measured the reconstructed pixel value and percentage standard deviation (%SD) of the same set-up as the previous experiment (phantom of 20 MBq in the FOV of the PET scanner and another phantom of 100 MBq positioned out-of-FOV). Neither scatter correction nor deadtime correction were applied for the reconstruction images. Fig. 6 shows average pixel counts and %SD for each slice. For slices 3–20 (farthest slices from the out-of-FOV activity), both average pixel counts and %SD increased with the out-of-FOV phantom.

The asymmetry of the slice sensitivity (average pixel counts) came from the scatter events from out-of-FOV activity; i.e., the slices (detector rings) closer to the out-of-FOV phantom were shaded by the internal fixed-shield of the PET scanner from the scatter events produced in the out-of-FOV phantom, while the slices (detector rings) farthest from the phantom were not effectively shaded. Also the decrease of the average counts in higher slices (~30–45: closer to the curtain-shield) with out-of-FOV phantom probably came from the increase of the singles deadtime. Using curtain-shield, the both average pixel counts and %SD slightly decreased meaning that scatter and random decreased.

B. Human Studies

To show the effectiveness of the curtain-shield in clinical situations, we measured the prompt minus delay (true*), random, and noise equivalent count (NEC) rates for FDG human volunteer studies (3D-acquisition mode). The true* in this measurement contains scatter because the scatter contribution is difficult

TABLE I
TRUE*, RANDOM, AND NEC RATES FOR FDG HUMAN STUDIES WITH AND WITHOUT THE CURTAIN-SHIELD FOR CHEST AND ABDOMINAL REGIONS

Region	Chest			Abdominal		
	True*	Random	NEC	True*	Random	NEC
Without shield	107 kcps	70.6 kcps	46.1 kcps	84.8 kcps	71.4 kcps	31.5 kcps
With shield	107 kcps	57.0 kcps	51.8 kcps	85.0k cps	59.4 kcps	35.5 kcps

to estimate and separate from the true*. The NEC rate is calculated by the following equation:

$$\text{NEC rate} = (\text{true}^*)^2/(\text{true}^* + 2 \text{ x random}).$$

This calculation overestimates the NEC rate for both without and with shield conditions because scatter is not included in the calculation and the true* contains scatter.

A subject was injected with 200 MBq of FDG. Measurements were started 50 min after injection. Measurements were made for the chest and abdominal regions, which are respectively affected by FDG accumulation in the brain and bladder.

Table I shows the true*, random, and NEC rates for FDG human studies with and without the curtain-shield. In the FDG studies in both chest and abdominal region imaging, random rates decreased approximately 20%. NEC rates increased 12% for the chest region and 13% for the abdominal region.

IV. DISCUSSION AND CONCLUSION

We developed and tested a curtain-shield. Because it is flexible, it could be used safely even in body studies.

In the experiments, the curtain-shield was only attached to the front region of the PET scanner. It can also be used on the back of the PET scanner. By using the curtain-shield on both sides of the PET scanner, the effectiveness (reduction of random and scatter) will be increased more although it is difficult to hang the shield at the back end of the detector ring.

For obese subjects, the curtain-shield might touch them and could be dragged into the scanner. This might decrease the sensitivity of the slices near the curtain-shield and may cause artifacts in the images. To avoid these problems, a solution is to reduce the length of the curtain-shield by folding it up at the joints of the tungsten plates before scanning because the joints of the curtain shield are flexible and easy to fold.

In Fig. 6(A), asymmetry distribution of the slice sensitivity (pixel counts) with out-of-FOV phantom was significant without scatter and deadtime corrections. Precise corrections are needed to correct the asymmetry distribution. The curtain-shield can improve the asymmetry distribution although the impact is not large.

Contributions from scatter and random events from out-of-FOV will be more serious for new PET scanners with longer axial FOV [7] and for PET/CT scanners with larger patient ports [8], [9]. In these PET systems, the developed curtain-shield will be more effective in random and scatter rejection.

ACKNOWLEDGMENT

The authors would like to thank the Matsuki Co. for manufacturing some parts of the curtain-shield.

REFERENCES

[1] S. Yamamoto, S. Miura, Y. Shouji, H. Iida, and I. Kanno, "Development of a front shield for a 3D positron emission tomography," *Kaku Igaku*, vol. 33, no. 6, pp. 641–646, 1996.

[2] T. J. Spinks, M. P. Miller, D. L. Bailey, P. M. Bloomfield, L. Livieratos, and T. Jones, "The effect of activity outside the direct field of view in a 3D-only whole-body positron tomography," *Phys. Med. Biol.*, vol. 43, no. 4, pp. 895–904, 1998.

[3] C. J. Thompson, S. Kecani, and S. Boelen, "Evaluation of a neck-shield for use during neurological studies with a whole-body PET scanner," *IEEE Trans. Nucl. Sci.*, vol. 48, no. 4, pp. 1512–1517, 2001.

[4] M. E. Daube Witherspoon, A. Belakhlef, S. L. Green, and I. Zanzi, "Design of patient shielding to reduce the effect of out-of-field radioactivity in 3D PET," in *IEEE Nuclear Science Symp., Conf. Rec.*, 1998, vol. 2, pp. 1237–1242.

[5] R. Boellaard, H. W. de Jong, C. F. Molthoff, F. Buijs, M. Lenox, R. Nutt, and A. A. Lammertsma, "Use of an in-field-of-view shield to improve count rate performance of the single crystal layer high-resolution research tomograph PET scanner for small animal brain scans.," *Phys. Med. Biol.*, vol. 48, no. 23, pp. N335–42, 2003.

[6] T. Hasegawa, H. Murayama, H. Matsuura, T. Yamaya, and S. Tanada, "Shielding effects of body-shields for 3D PET," *Igaku Butsuri.*, vol. 22, no. 4, pp. 318–326, 2002.

[7] S. Surti and J. S. Karp, "Imaging characteristics of a 3-dimensional GSO whole-body PET camera," *J. Nucl. Med.*, vol. 45, no. 6, pp. 1040–1049, 2004.

[8] O. Mawlawi, D. A. Podoloff, S. Kohlmyer, J. J. Williams, C. W. Stearns, R. F. Culp, and H. Macapinlac, "Performance characteristics of a newly developed PET/CT scanner using NEMA standards in 2D and 3D mode," *J. Nucl. Med.*, vol. 45, no. 10, pp. 1734–1742, 2004.

[9] Y. E. Erdi, S. A. Nehmeh, T. Mulnix, J. L. Humm, and C. C. Watson, "PET performance measurements for an LSO-based combined PET/CT scanner using the National Electrical Manufacturers Association NU 2-2001 standard," *J. Nucl. Med.*, vol. 45, no. 5, pp. 813–21, 2004.

ORIGINAL ARTICLE

Brain Serotonin Transporter Density and Aggression in Abstinent Methamphetamine Abusers

Yoshimoto Sekine, MD, PhD; Yasuomi Ouchi, MD, PhD; Nori Takei, MD, PhD, MSc; Etsuji Yoshikawa, BA; Kazuhiko Nakamura, MD, PhD; Masami Futatsubashi, BA; Hiroyuki Okada, BA; Yoshio Minabe, MD, PhD; Katsuaki Suzuki, MD, PhD; Yasuhide Iwata, MD, PhD; Kenji J. Tsuchiya, MD; Hideo Tsukada, PhD; Masaomi Iyo, MD, PhD; Norio Mori, MD, PhD

Context: In animals, methamphetamine is known to have a neurotoxic effect on serotonin neurons, which have been implicated in the regulation of mood, anxiety, and aggression. It remains unknown whether methamphetamine damages serotonin neurons in humans.

Objective: To investigate the status of brain serotonin neurons and their possible relationship with clinical characteristics in currently abstinent methamphetamine abusers.

Design: Case-control analysis.

Setting: A hospital research center.

Participants: Twelve currently abstinent former methamphetamine abusers (5 women and 7 men) and 12 age-, sex-, and education-matched control subjects recruited from the community.

Interventions: The brain regional density of the serotonin transporter, a structural component of serotonin neurons, was estimated using positron emission tomography and *trans*-1,2,3,5,6,10-beta-hexahydro-6-[4-(methylthio) phenyl]pyrrolo-[2,1-a]isoquinoline ([^{11}C](+)McN-5652). Estimates were derived from region-of-interest and statistical parametric mapping methods, followed by within-case analysis using the measures of clinical variables.

Main Outcome Measures: The duration of methamphetamine use, the magnitude of aggression and depressive symptoms, and changes in serotonin transporter density represented by the [^{11}C](+)McN-5652 distribution volume.

Results: Methamphetamine abusers showed increased levels of aggression compared with controls. Region-of-interest and statistical parametric mapping analyses revealed that the serotonin transporter density in global brain regions (eg, the midbrain, thalamus, caudate, putamen, cerebral cortex, and cerebellum) was significantly lower in methamphetamine abusers than in control subjects, and this reduction was significantly inversely correlated with the duration of methamphetamine use. Furthermore, statistical parametric mapping analyses indicated that the density in the orbitofrontal, temporal, and anterior cingulate areas was closely associated with the magnitude of aggression in methamphetamine abusers.

Conclusions: Protracted abuse of methamphetamine may reduce the density of the serotonin transporter in the brain, leading to elevated aggression, even in currently abstinent abusers.

Arch Gen Psychiatry. 2006;63:90-100

Author Affiliations: Department of Psychiatry and Neurology, Hamamatsu University School of Medicine, Hamamatsu, Japan (Drs Sekine, Takei, Nakamura, Minabe, Suzuki, Iwata, Tsuchiya, and Mori); Positron Medical Center, Hamamatsu Medical Center, Hamakita, Japan (Dr Ouchi); Division of Psychological Medicine, Institute of Psychiatry, London, England (Dr Takei); Central Research Laboratory, Hamamatsu Photonics KK, Hamakita (Dr Tsukada and Messrs Yoshikawa, Futatsubashi, and Okada); and Department of Psychiatry, Chiba University Graduate School of Medicine, Chiba, Japan (Dr Iyo).

METHAMPHETAMINE IS A powerfully addictive drug, and the number of its abusers has been steadily increasing worldwide.[1-5] Long-term methamphetamine abuse can produce various psychiatric symptoms, including psychosis, depression, anxiety, and aggression, under conditions of intoxication and withdrawal.[6,7] These psychiatric states are sometimes prolonged, in the form of residual symptoms, and are easily exacerbated in some long-term abusers by methamphetamine reuse or by psychological stress.[3,8-10]

In animal studies, the biochemical effects of the neurotoxicity of methamphetamine on mature neurons, especially on the dopaminergic and serotonergic axon arbors, are well documented,[11,12] although neurotoxic methamphetamine may also cause cell death through apoptosis or necrosis.[12,13] However, methamphetamine-induced neuronal damage is thought to vary across species.[14,15] For example, in contrast to the findings in rats,[11] which indicate that serotonergic neurons are more sensitive to the methamphetamine-induced toxicity than are dopaminergic neurons, recent findings[16] have suggested that serotonergic neurons in nonhuman primates seem to be less affected by methamphetamine administration than are dopaminergic neurons.

In vivo studies using positron emission tomography (PET) are helpful for understanding the contribution of methamphetamine neurotoxicity and induced

Table 1. Demographic and Clinical Characteristics of the 24 Study Participants

	Control Subjects (n = 12)		Methamphetamine Abusers (n = 12)*	
	Mean ± SD	Range	Mean ± SD	Range
Age, y	31.8 ± 6.6	21-44	31.4 ± 6.8	21-44
Education, y	11.5 ± 1.2	9-12	11.1 ± 2.1	9-12
Duration of methamphetamine use, y	NA	NA	6.7 ± 3.2	1.5-11.0
Duration of methamphetamine abstinence, y	NA	NA	1.6 ± 1.3	0.5-5.0
BPRS positive symptoms subscale score	NA	NA	5.3 ± 3.9	0-14
BPRS negative symptoms subscale score	NA	NA	0.0 ± 0.0	0.0
17-Item HAM-A score	NA	NA	3.8 ± 6.3	0-16
17-Item HAM-D score	NA	NA	4.0 ± 6.3	0-19
Scale for methamphetamine craving score	NA	NA	4.9 ± 3.4	1-10
Aggression Questionnaire score†	30.2 ± 1.7	29-34	75.0 ± 13.9‡	46-97

Abbreviations: BPRS, Brief Psychiatric Rating Scale; HAM-A, Hamilton Rating Scale for Anxiety; HAM-D, Hamilton Rating Scale for Depression; NA, not applicable.
*All the abusers took methamphetamine intravenously.
†Higher scores represent greater aggression.
‡Significantly difference from control subjects using the *t* test ($P<.001$).

neural damage to the long-term withdrawal syndrome. Recent PET studies have shown that long-term use of methamphetamine decreases the density of DA transporters, which are located on dopaminergic terminals in the human brain[1-3,17,18]; moreover, long-term use of methamphetamine may cause severe positive symptoms (eg, delusions and hallucinations) and an increased reduction in DA transporter density.[3,18] However, to date, no studies have addressed the alteration of serotonergic neurons in methamphetamine abusers. In addition, it is not known whether such changes, if found, could be related to the psychiatric symptoms frequently observed in currently abstinent methamphetamine abusers.

We, therefore, examined the possibility of changes in the density of the serotonin transporter, an index of serotonin neuronal damage,[19-25] in methamphetamine abusers by means of PET. This information was then considered as part of an evaluation of the potential associations between serotonin transporter density and participant clinical characteristics.

METHODS

PARTICIPANTS

The ethics committees of the Hamamatsu University School of Medicine and Hamamatsu Medical Center approved this study. Written informed consent was obtained from each participant after they were provided an explanation of the study procedures. Twelve currently abstinent methamphetamine abusers who had previously abused only methamphetamine (ie, monodrug abusers) and 12 age-, sex-, and education-matched control subjects participated in this study (**Table 1**). Potential participants were recruited from the community by means of poster advertisements and word of mouth in and around Hamamatsu City, which is located in the middle of the mainland of Japan. The participants in the methamphetamine group were required to attend a weekly meeting at the Drug Detoxification and Rehabilitation Program Center of Hattori Mental Hospital (Iwata, Japan) to maintain and ensure abstinence until the PET study was conducted.

All the methamphetamine abusers had used the drug recreationally and had no history of toxic or high-dose methamphetamine use. None of the abusers had any history of hospitalization or treatment at psychiatric hospitals. We assessed the participants regarding the use of other illicit drugs, including (±)3,4-methylenedioxymethamphetamine, cocaine, cannabis, heroin, and toluene, because these substances are known to cause psychiatric symptoms and to affect neural transmission in the brain.[19,26,27] However, none of the methamphetamine abusers recruited for the present study were found to have a history of such illicit drug use. All the methamphetamine abusers were naive to neuropsychiatric medications, such as antipsychotics and antidepressants. None of the methamphetamine abusers had a history of psychiatric disorders, including antisocial or intermittent explosive disorder, or a history of increased aggression before the use of methamphetamine. The controls were healthy and had never used methamphetamine or any other illicit drugs, and none of them met any of the relevant criteria according to the *Diagnostic and Statistical Manual of Mental Disorders, Fourth Edition*.[28] The control and methamphetamine groups showed similar habits of occasional drinking and smoking, but none of the participants fulfilled either the alcohol- or the nicotine-related *Diagnostic and Statistical Manual of Mental Disorders, Fourth Edition* criteria. These evaluations were determined using the Structured Clinical Interview for the *Diagnostic and Statistical Manual of Mental Disorders, Fourth Edition*.[29] To increase the accuracy of the abusers' profiles, detailed information on the duration of methamphetamine use and the history of psychiatric symptoms was retrospectively obtained using Structured Clinical Interview for the *Diagnostic and Statistical Manual of Mental Disorders, Fourth Edition*–based interviews with the abusers and their family members. The period of methamphetamine use was defined as the duration between the first and last use. When intervals of abstinence longer than 1 month occurred during the duration of methamphetamine use as defined, these intervals were subtracted from the total duration value. The methamphetamine abstinence period was arbitrarily defined as the duration between the day of the last use of methamphetamine and that of the PET examination.

DRUG SCREENING

During the weekly meeting at the Drug Detoxification and Rehabilitation Program Center, the absence of recent methamphetamine and other drug use was regularly confirmed using a rapid

immunoassay for the qualitative detection of the metabolites of the following 8 classes of drugs: amphetamines, including methamphetamine and (±)3,4-methylenedioxymethamphetamine; barbiturates; benzodiazepines; cocaine; methadone; opiates; tetrahydrocannabinol; and tricyclic antidepressants (Triage8; Biosite Diagnostics, San Diego, Calif). In addition, the participants were tested for urinary hippuric acid, a biomarker of toluene use, using high-performance liquid chromatography according to the standard diagnostic methods.[27] These assessments were also performed on the same day as the PET examination. When necessary, we assessed hair samples using high-performance liquid chromatography, which enabled us to verify long periods of methamphetamine abstinence.[30]

CLINICAL EVALUATION

The severity of psychiatric symptoms in methamphetamine abusers was evaluated using the Aggression Questionnaire (AQ)[31]; the scores can range from 29 to 145, with higher scores representing greater aggression. In addition, the 17-item Hamilton Rating Scale for Anxiety,[32] the 17-item Hamilton Rating Scale for Depression,[33] and positive and negative symptom subscores[34] on the Brief Psychiatric Rating Scale[35] were included in the evaluation. The Subjective Drug Effect Rating Scale for Cocaine[36] was modified and used for the assessment of cravings for methamphetamine. The scores on this assessment can range from 1 to 10, with higher scores representing more intense craving sensations (Table 1). These evaluations were performed on the day of the PET examination by a trained research psychiatrist masked to the PET results.

MAGNETIC RESONANCE IMAGING AND MAGNETIC RESONANCE IMAGING–TO-PET COORDINATE PROCEDURES

Three-dimensional magnetic resonance imaging (MRI) was performed just before the PET examination using a 0.3-T MRI unit (MRP7000AD; Hitachi Medical Corp, Tokyo, Japan) and the following acquisition parameters: repetition time, 200 milliseconds; echo time, 23 milliseconds; flip angle, 75°; slice thickness, 2 mm with no gap; and matrix, 256 × 256. In reference to the measurements of the tilt angle and spatial coordinates obtained in the procedure for determining the anterior-posterior intercommissural line on each participant's sagittal MRIs, a PET gantry was set parallel to the anterior-posterior intercommissural line by tilting and moving the gantry for each participant, which permitted reconstruction of the PET images parallel to the anterior-posterior intercommissural line without reslicing; using this approach, we allocated regions of interest (ROIs) on the target areas of the original PET images.[37]

PET PROCEDURES

We used a high-resolution brain PET scanner (model SHR12000; Hamamatsu Photonics KK, Hamamatsu, Japan), which was capable of yielding 47 PET images simultaneously.[38] Before dynamic scanning, a 20-minute transmission scan was performed for attenuation correction using a germanium Ge 68/gallium Ga 68 source with the participant's head fixed by means of a radiosurgery-purpose thermoplastic face mask. Then, after a bolus intravenous injection of a 370-MBq dose of *trans*-1,2,3,5,6,10-beta-hexahydro-6-[4-(methylthio)phenyl]pyrrolo-[2,1-a]isoquinoline ([^{11}C](+)McN-5652), a ligand with high specificity to serotonin transporter,[21,39] 38 serial PET scans (time frames: 4 × 60, 20 × 120, and 14 × 300 seconds) were performed for 92 minutes. A total of 23 arterial blood samples were collected at intervals of 10 seconds to 15 minutes after the tracer injection. The blood samples were analyzed using thin-layer chromatography (Whatman AL SIL G/UV 20 × 20 cm; Whatman Japan KK, Tokyo) and a storage phosphorscreen bioimaging analyzer (model BAS-1500; Fuji Photo Film Co, Tokyo) to determine the levels of unmetabolized tracer.

IMAGE ANALYSIS AND KINETIC MODELING

At the beginning of the study, the MRI voxel size was adjusted to the PET voxel size 3-dimensionally using image processing software (DrView; Asahi Kasei Co, Tokyo) on a Sun workstation (HyperSPARC ss-20; Sun Microsystems, Santa Clara, Calif). These reformatted MRIs with 3-dimensional scales and coordinates identical to those of the PET images were used as anatomic landmarks for the ROI setting, which allowed for minimization of the partial volume effects.[3,18,40,41] An investigator masked to the participant's condition placed 10 ROIs bilaterally over the midbrain, thalamus, caudate nucleus, putamen, amygdala, anterior cingulate cortex, dorsolateral prefrontal cortex, orbitofrontal cortex, temporal cortex, and cerebellar cortex on the MRIs, as previously described.[40,42,43] After delineation of the ROIs was completed on the reformatted MRIs, the PET images were displayed side-by-side with the MRIs. Then, the determined ROIs were placed on the same area on the MRIs and the corresponding PET images.

To assess the brain serotonin transporter density, we analyzed the [^{11}C](+)McN-5652 binding data on the basis of a model that described the radioligand kinetics using a single-tissue compartment and 3 parameters—uptake of radioligand in brain tissue (K_1), release of radioligand from brain tissue (k_2), and blood volume—because the regional brain [^{11}C](+)McN-5652 distribution volume (DV) (ie, the ratio of K_1/k_2) estimated by this model is known to correlate with the known regional brain serotonin transporter density[21,39,44] and has been reported to be suitable for evaluating amphetamine-induced serotonergic neurotoxicity.[21] Cerebral radioactivity was corrected for the contribution of plasma radioactivity, assuming a 5% blood volume in the ROIs. The K_1 and k_2 values were estimated by fitting the metabolite-corrected plasma time–radioactivity curves and the blood volume–corrected brain time–radioactivity curves using a nonlinear least squares algorithm.[3,18,40]

STATISTICAL ANALYSIS

In addition to the ROI method described in the "Methods" section, we also performed a voxel-based whole-brain analysis using statistical parametric mapping (SPM) software (SPM99; Wellcome Department of Cognitive Neurology, Institute of Neurology, London). Based on the same kinetic model as that used for the ROI method, absolute parametric [^{11}C](+)McN-5652 DV images were generated for each participant using biomedical image quantification and kinetic modeling software (PMOD version 2.5; PMOD Technologies Ltd, Zurich, Switzerland) (**Figure 1**).[45,46] To normalize the absolute DV image to the standard stereotaxic brain atlas,[47] we used transformation parameters for early integrated images of [^{11}C](+)McN-5652 (0-20 minutes after injection).[48,49] Subsequently, *t* statistics were performed on a voxel-by-voxel basis (voxel size: 2.0 × 2.0 × 2.0 mm), resulting in *t* statistic maps. Then, the results were transformed to the unit normal distribution. For the SPM analysis, we assessed both group differences in the regional [^{11}C](+)McN-5652 DVs and the possible relationship between the regional changes in [^{11}C](+)McN-5652 DVs and the severity of clinical symptoms in methamphetamine abusers. Age and sex were treated as covariates, and the scores on the clinical measures (AQ, Hamilton Rating Scale for Anxiety, Hamilton Rating Scale for Depression, positive and negative symptoms on

the Brief Psychiatric Rating Scale, and the scale for methamphetamine craving) were considered to be variables of interest. To test hypotheses about the regional specific effects of these variables, the estimates were compared using 2 linear contrasts (positive or negative correlation). According to recently published PET studies[6,50] of methamphetamine abusers, the level of significance was determined using a voxel height threshold of $P=.05$ (corrected). The cluster significance threshold was also set at $P=.05$ (corrected).

To compare the mean values of the demographic and clinical variables in control subjects and methamphetamine abusers, an unpaired t test was used. We tested the main effect of methamphetamine use on [^{11}C](+)McN-5652 DVs derived from 10 brain regions using multivariate analysis of variance. Statistical significance was set at $P<.05$. To investigate the correlation between the [^{11}C](+)McN-5652 DV and the clinical variables in methamphetamine abusers, including the duration of methamphetamine use and abstinence, the Pearson correlation coefficient was computed, with age and sex adjusted for; after applying the Bonferroni correction, the level of statistical significance was set at $P=.005$ (SPSS version 11.0J; SPSS Japan Inc, Tokyo).

RESULTS

PSYCHIATRIC STATES OF ABSTINENT METHAMPHETAMINE ABUSERS

Methamphetamine abusers showed no apparent negative symptoms as demonstrated by Brief Psychiatric Rating Scale assessment (Table 1). All methamphetamine abusers had previously experienced psychosis during methamphetamine use. Two methamphetamine abusers had persistent psychotic symptoms, such as persecutory delusions and auditory hallucinations; 5 had a depressed mood; 4 had anxiety; 4 showed severe aggression; and 4 had no psychiatric symptoms except for aggressive behavior. The mean AQ score was significantly higher in methamphetamine abusers than in controls ($t=-11.1$; $P<.001$).

ROI ANALYSIS

The traditional ROI-based analysis showed that methamphetamine abusers had significantly decreased [^{11}C](+)McN-5652 DVs in their global brain regions compared with control subjects (Wilks $\Lambda=0.001$; $P=.003$) (**Figure 2**). Subsequent univariate analysis of variance revealed that methamphetamine abusers had significantly lower [^{11}C](+)McN-5652 DVs than control subjects in all 10 ROIs studied ($P<.001$ for all). There was no group × sex interaction effect in the [^{11}C](+)McN-5652 DV, indicating no sex-specific effect in [^{11}C](+)McN-5652 DVs (Wilks $\Lambda=0.47$; $P=.37$).

Figure 3 shows the correlations between [^{11}C](+)McN-5652 DVs and clinical variables in methamphetamine abusers. The [^{11}C](+)McN-5652 DVs in 5 of the 10 ROIs (ie, the midbrain, thalamus, caudate nucleus, putamen, and orbitofrontal cortex) significantly correlated negatively with the duration of methamphetamine use ($P<.005$ for all by Pearson correlation coefficient) (Figure 3A). There was no correlation in any of the 10 ROIs between [^{11}C](+)McN-5652 DVs and the duration of methamphetamine abstinence, which lasted 6 months to 5 years in our participants (Figure 3B). The magnitude of aggression, as assessed using the AQ, increased significantly with decreasing [^{11}C](+)McN-5652 DVs in 8 of the 10 ROIs (ie, the thalamus, caudate nucleus, putamen, anterior cingulate cortex, temporal cortex, orbitofrontal cortex, dorsolateral prefrontal cortex, and cerebellar cortex) ($P<.005$ for all by Pearson correlation coefficient) (Figure 3C). Other clinical variables, including craving, were not statistically significantly correlated with changes in [^{11}C](+)McN-5652 DVs (data not shown).

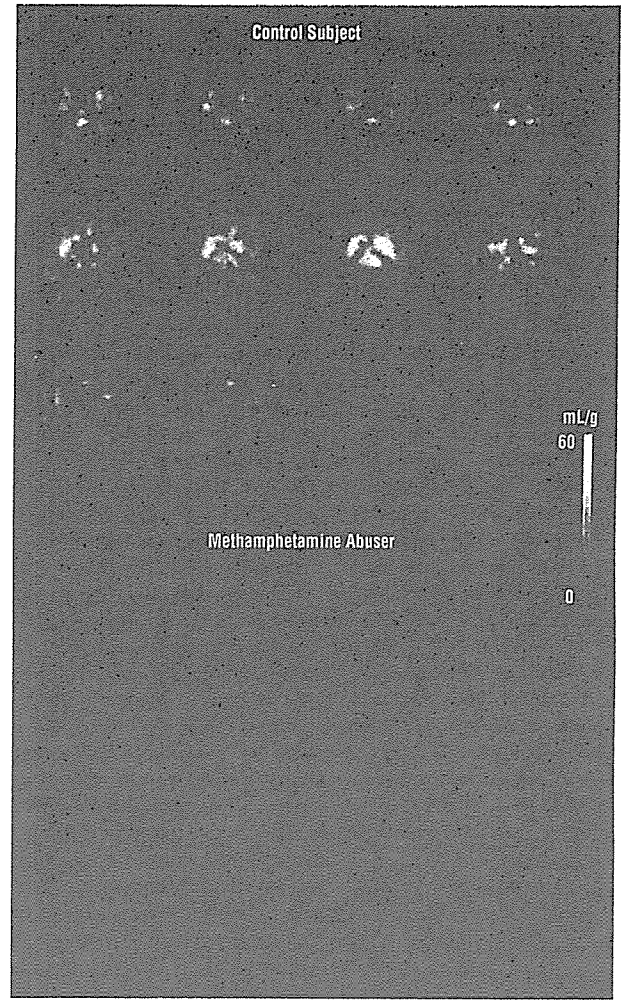

Figure 1. Voxel-based *trans*-1,2,3,5,6,10-beta-hexahydro-6-[4-(methylthio) phenyl]pyrrolo-[2,1-a]isoquinoline ([^{11}C](+)McN-5652) distribution volume images from a control subject and a methamphetamine abuser. These absolute parametric images were normalized to the standard stereotaxic brain atlas using transformation parameters for early integrated images of [^{11}C](+)McN-5652 (0-20 minutes after injection). The [^{11}C](+)McN-5652 distribution volumes in broad areas of the brain of the methamphetamine abuser were lower than those of the control subject.

SPM ANALYSIS

Figure 4 illustrates the results of the whole-brain voxel-based SPM analysis of [^{11}C](+)McN-5652 DVs. Figure 4A shows that the methamphetamine group had widely distributed reductions in [^{11}C](+)McN-5652 DVs compared with the control group ($P<.05$, corrected) (**Table 2**). In accord with the findings derived from the ROI analysis, the SPM analysis revealed an extensive clus-

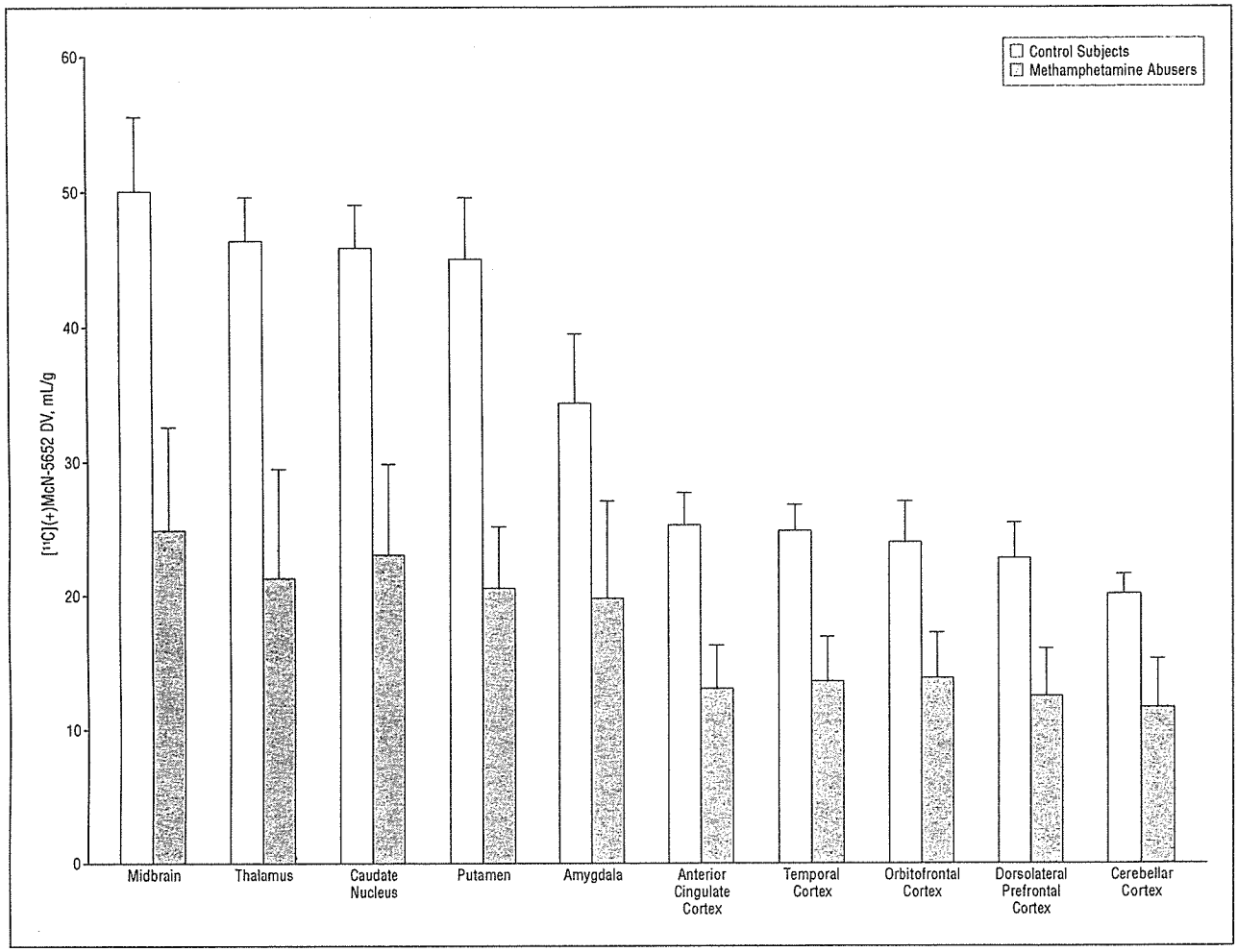

Figure 2. Mean regional brain *trans*-1,2,3,5,6,10-beta-hexahydro-6-[4-(methylthio)phenyl]pyrrolo-[2,1-a]isoquinoline ([^{11}C](+)McN-5652) distribution volumes (DVs) in control subjects and methamphetamine abusers. Methamphetamine abusers had significantly decreased [^{11}C](+)McN-5652 DVs in the global regions compared with controls (Wilks $\Lambda = 0.001$; $P = .003$, by multivariate analysis of variance). Univariate analysis of variance revealed that methamphetamine users had significantly lower [^{11}C](+)McN-5652 DVs than controls in all regions studied ($P < .001$ for all). Error bars represent SE.

ter of voxels with reduced [^{11}C](+)McN-5652 DVs occupying the right insular area and extending out into the bilateral putamen, caudate, thalamus, hypothalamus, midbrain, temporal, parietal, frontal, occipital, cerebellar, anterior cingulate, and posterior cingulate areas. This cluster consisted of 45 315 voxels (363 mL). Figure 4B shows clusters in which the magnitude of aggression increased significantly with decreasing [^{11}C](+)McN-5652 DVs. These clusters were located on the bilateral orbitofrontal areas ($P \leq .001$), left inferior temporal area ($P < .001$), and right anterior cingulate gyrus area ($P < .001$) (**Table 3**). The other clinical variables did not reach statistical significance (data not shown).

COMMENT

In the present study, methamphetamine abusers had statistically significantly decreased [^{11}C](+)McN-5652 DVs, a representative measure of serotonin transporter density,[21,39,44] in their global brain regions compared with control subjects. The finding of significantly reduced [^{11}C](+)McN-5652 DVs in a several brain regions in methamphetamine abusers, as revealed using the ROI approach, was in accord with the results of voxel-based SPM analysis. In addition, there was no group × sex interaction effect in terms of the [^{11}C](+)McN-5652 DV, indicating that abnormal [^{11}C](+)McN-5652 DVs in the brains of methamphetamine abusers are observed in both sexes. These findings suggest that the ingestion of methamphetamine leads to a global and severe reduction in the density of human brain serotonin transporters.

The values of the density of serotonin transporters in widely distributed brain regions, including the midbrain, hypothalamus, thalamus, caudate, putamen, amygdala, temporal cortex, and occipital cortex, were found to negatively correlate with the duration of methamphetamine use. This result implies that the longer methamphetamine is used, the more severe the decrease in serotonin transporter density will be. Although the duration of methamphetamine use is viewed as a proxy measure for the actual amount of intake of the drug, such a relationship in a dose-response manner strongly suggests a link between the use of methamphetamine and damage to serotonin neurons. This is compatible with the results of animal experiments[51] demonstrating dose-dependent methamphetamine-induced serotonin transporter reduction.